ANL-19/06

Argonne NATIONAL LABORATORY

Validation of Gamma Dose Rate Calculation Methodology using the Morris and Turkey Point Measurements

Nuclear Science and Engineering Division

ANL-19/06

Validation of Gamma Dose Rate Calculation Methodology using the Morris and Turkey Point Measurements

Yan Cao and Bo Feng
Nuclear Science and Engineering Division
Argonne National Laboratory

January 24, 2019

Validation of Gamma Dose Rate Calculation Methodology using the Morris and Turkey Point Measurements

Table of Contents

Page

ABSTRACT 1

1. INTRODUCTION 2

2. DESCRIPTION OF THE EXPERIMENTAL SETUP 3

A. MORRIS EXPERIMENTAL SETUP 3

B. TURKEY POINT EXPERIMENTAL SETUP 7

3. NUMERICAL MODES AND NUMERICAL SIMULATIONS 11

A. NUMERICAL MODELS AND ANALYSIS FOR THE MORRIS EXPERIMENTS 11

B. NUMERICAL MODELS AND ANALYSIS FOR THE TURKEY POINT EXPERIMENTS 23

4. RESULTS COMPARISON AND EXPERIMENTAL VALIDATIONS 29

A. MORRIS EXPERIMENTS SIMULATION RESULTS AND COMPARISON 29

B. TURKEY POINT EXPERIMENTS SIMULATION RESULTS AND COMPARISON 31

5. SUMMARY AND FUTURE WORK 38

REFERENCES 41

Validation of Gamma Dose Rate Calculation Methodology using the Morris and Turkey Point Measurements

List of Figures

Page

FIGURE 1. (A) MORRIS EXPERIMENTAL SETUP. (B) ION CHAMBER LOCATIONS RELATIVELY TO THE FUEL BUNDLE. (C) X-Y CUT VIEW OF THE EXPERIMENTAL SETUP. 7

FIGURE 2. (A) FUEL ASSEMBLY B03 IN THE HOT CELL FOR MEASUREMENTS. (B) TLD DETECTOR LOCATIONS RELATIVE THE FUEL ASSEMBLY. (C) TURKEY POINT FUEL ASSEMBLY REFERENCE SCHEME. 9

FIGURE 3. MONTE CARLO MODEL OF THE FUEL ASSEMBLIES FOR THE WESTINGHOUSE 14X14 FUEL ASSEMBLIES. 12

FIGURE 4. MONTE CARLO CALCULATED REACTIVITIES IN THE FUEL BURNUP SIMULATIONS FOR THE 1A FUEL BUNDLE USING THE MCNP6, MCODE AND THE SERPENT CODE RESPECTIVELY. 13

FIGURE 5. MONTE CARLO CALCULATED AMOUNT OF ACTINIDE ISOTOPE AT THE END OF THE FUEL BURNUP SIMULATIONS FOR THE 1A FUEL BUNDLE USING THE MCNP6, MCODE AND THE SERPENT CODE RESPECTIVELY. 13

FIGURE 6. MONTE CARLO CALCULATED AMOUNT OF FISSION ISOTOPES AT THE END OF THE FUEL BURNUP SIMULATIONS FOR THE 1A FUEL BUNDLE USING THE MCNP6, MCODE AND THE SERPENT CODE RESPECTIVELY. 13

FIGURE 7. THE CALCULATED GAMMA SOURCE ENERGY SPECTRUM OF THE 1A SPENT FUEL BUNDLE AFTER 4 YEARS OF COOLING USING THE SERPENT CODE AND MCODE FOR FUEL BURNUP ANALYSIS. 15

FIGURE 8. THE CALCULATED GAMMA SOURCE ENERGY SPECTRUM FROM DIFFERENT GAMMA SOURCES FOR THE 1A SPENT FUEL BUNDLE AFTER 4 YEARS OF COOLING. 17

FIGURE 9. MCNP MODEL OF THE MORRIS EXPERIMENTAL SETUP WITH FUEL BUNDLE 1A. 18

FIGURE 10. COMPARISON OF THE CALCULATED GAMMA DOSE RATES WITH DIFFERENT OPEN WIDTH OF THE TUBE SLOT FOR FUEL BUNDLE 1A. 19

FIGURE 11. COMPARISON OF THE CALCULATED GAMMA DOSE RATE WITH DIFFERENT HEIGHT AND DIAMETER OF THE DIVING BELL FOR FUEL BUNDLE 1A. 21

FIGURE 12. COMPARISON OF THE CALCULATED GAMMA DOSE RATE WITH DIFFERENT AIR PRESSURE AND WATER LEVEL INSIDE THE DIVING BELL FOR FUEL BUNDLE 1A. 22

FIGURE 13. AXIAL GAMMA SOURCE DISTRIBUTIONS TESTED IN THE MONTE CARLO TRANSPORT SIMULATIONS FOR FUEL BUNDLE 1A. 22

FIGURE 14. COMPARISON OF THE CALCULATED GAMMA DOSE RATE RATIOS (MCNP MODEL VALUE VS EXPERIMENT DATA) WITH THE THREE AIXAL FUEL BURNUP DISTRIBUTIONS FOR FUEL BUNDLE 1A. 23

FIGURE 15. COMPARISON OF THE CALCULATED GAMMA DOSE WITH DIFFERENT FLUX-TO-DOSE CONVERSION FACTORS FOR FUEL BUNDLE 1A. 23

FIGURE 16. MONTE CARLO MODEL OF THE FUEL ASSEMBLIES FOR THE WESTINGHOUSE 15X15 FUEL ASSEMBLIES. 24

FIGURE 17. SERPENT CALCULATED REACTIVITY LOSSES DURING THE FUEL BURNUP FOR THE TURKEY POINT FUEL ASSEMBLY B03 AND D04. 25

FIGURE 18. CALCULATED GAMMA SOURCE SPECTRA FROM THE DECAY OF FISSION PRODUCTS, DECAY OF CO-60 IN THE SPRING AND SPACER FOR TURKEY POINT FUEL ASSEMBLY B03. 27

FIGURE 19. MCNP MODEL OF THE TURKEY POINT EXPERIMENTS TO (A) REVIEW GRAPH SHOWING THE HORIZONTAL ALUMINUM TUBE AND THE THE DETECTORS (B) REVIEW GRAPH SHOWING THE VERTICAL ALUMINUM TUBE AND THE DETECTORS. 28

FIGURE 20 COMPARISON OF THE CALCULATED GAMMA DOSE RATE RATIOS TO THE MEASURED VALUES FOR FUEL BUNDLE 1A, 2A, 2B AND 2D IN THE MORRIS EXPERIMENTS. 30

FIGURE 21 COMPARISON OF THE CALCULATED GAMMA DOSE RATES AND THE MEASURED VALUES FOR DETECTORS INSIDE THE INSTRUMENTATION TUBE OF THE FUEL ASSEMBLY B03. 34

FIGURE 22 COMPARISON OF THE CALCULATED GAMMA DOSE RATES AND THE MEASURED VALUES FOR DETECTORS INSIDE THE GUIDE TUBE OF THE FUEL ASSEMBLY B03. 34

FIGURE 23 COMPARISON OF THE CALCULATED GAMMA DOSE RATES AND THE MEASURED VALUES FOR DETECTORS CONTACTING THE B03 FUEL ASSEMBLY SURFACE. 34

FIGURE 24 COMPARISON OF THE CALCULATED GAMMA DOSE RATES AND THE MEASURED VALUES FOR DETECTORS ONE FOOT ABOVE THE FUEL ASSEMBLY B03. 35

FIGURE 25 COMPARISON OF THE CALCULATED GAMMA DOSE RATES AND THE MEASURED VALUES FOR DETECTORS VERTICALLY PERPENDICULAR TO THE FUEL ASSEMBLY B03. 35

FIGURE 26 COMPARISON OF THE CALCULATED GAMMA DOSE RATES AND THE MEASURED VALUES FOR DETECTORS ONE FOOT ABOVE THE FUEL ASSEMBLY D04. 36

FIGURE 27 COMPARISON OF THE CALCULATED GAMMA DOSE RATES AND THE MEASURED VALUES FOR DETECTORS CONTACTING THE D04 FUEL ASSEMBLY SURFACE. 37

FIGURE 28 COMPARISON OF THE CALCULATED GAMMA DOSE RATES AND THE MEASURED VALUES FOR DETECTORS VERTICALLY PERPENDICULAR TO THE FUEL ASSEMBLY D04. 37

Validation of Gamma Dose Rate Calculation Methodology using the Morris and Turkey Point Measurements

List of Tables

Page

TABLE 1 SPECIFICATIONS OF THE MORRIS FUEL BUNDLE 1A, 2A, 2B AND 2D AND TURKEY POINT FUEL ASSEMBLY B03 AND D04. 4

TABLE 2 SPATIAL LOCATIONS OF THE ION CHAMBERS FOR MORRIS UNIT 1 AND 2 FUEL ASSEMBLIES. 5

TABLE 3 MEASURED GAMMA DOSE RATES FOR MORRIS UNIT 1 AND UNIT 2 FUEL ASSEMBLIES. 5

TABLE 4 MEASURED AXIAL DISTRIBUTIONS OF THE DOSE RATES FOR FUEL ASSEMBLY B03. 10

TABLE 5 MEASURED AXIAL DISTRIBUTIONS OF THE DOSE RATES FOR FUEL ASSEMBLY D04. 10

TABLE 6 MEASURED RADIAL DISTRIBUTIONS OF THE GAMMA DOSE RATES FOR THE TURKEY POINT FUEL ASSEMBLY B03 AND D04. 11

TABLE 7 CALCULATED GAMMA RAY SOURCE CONTRIBUTIONS FROM THE RADIOISOTOPES IN THE MORRIS DISCHARGED FUEL ASSEMBLY 1A AT DISCHARGE AND AFTER 4 YEARS OR 30 YEARS OF COOLING. 15

TABLE 8 ESTIMATED CO IMPURITIES IN THE MORRIS FUEL ASSEMBLIES. 16

TABLE 9 MCNP TALLIED NEUTRON CROSS SECTIONS FOR CO-59 IN THE MORRIS OPERATION AT DIFFERENT FUEL BURNUP STEPS. 16

TABLE 10 MCNP MODEL ASSUMPTIONS AND PARAMETRIC STUDIES FOR FUEL BUNDLE 1A. 18

TABLE 11 MONTE CARLO CALCULATED CO-59 TRANSMUTATION AND CO-60 PRODUCTION IN THE TURKEY POINT FUEL ASSEMBLY B03 AND D04. 25

TABLE 12 DEFAULT 18-ENERGY GROUP STRUCTURES FOR GAMMA SPECTRA IN ORIGEN-S CODE. 26

TABLE 13 MCNP CALCULATED GAMMA DOSE RATES FOR THE FOUR FUEL BUNDLES IN THE MORRIS EXPERIMENTS. 29

TABLE 14 CALCULATED AXIAL GAMMA DOSE RATES FOR FUEL ASSEMBLY B03. 31

TABLE 15 CALCULATED RADIAL GAMMA DOSE RATES FOR THE FUEL ASSEMBLY B03 AND D04. 31

TABLE 16 CALCULATED AXIAL GAMMA DOSE RATES FOR FUEL ASSEMBLY D04. 32

TABLE 17 CALCULATED THE GAMMA DOSE RATES FROM THE GAMMA RAY SOURCES FOR DETECTORS LOCATED ABOUT 11 FEET FROM THE REFERENCE POINT IN THE INSTRUMENT TUBE, GUIDE TUBE AND TUBE ON THE ASSEMBLY SURFACE RESPECTIVELY. 33

Validation of Gamma Dose Rate Calculation Methodology using the Morris and Turkey Point Measurements

Abstract

The ability to accurately predict the dose rates from the spent nuclear fuel assembly is very important for determining whether the used nuclear fuel is self-guarded and self-protected. Studies have shown that the direct numerical calculations of the dose rates gave a much lower value than a typical reference. This report summarizes the benchmark studies performed to evaluate the numerical methodologies used in calculating the gamma dose rates of the spent nuclear fuel assemblies. The Morris and Turkey Point experimental data for dose rates measured through air were used in the analyses. Numerical simulations of the gamma dose rate measurements included the fuel depletion analysis of the fuel assembly as well as its structural materials irradiated inside the reactor core, the radioisotopes decay, and photon transport simulations to calculate the gamma dose rates. The different factors which affect the calculated gamma dose rates were addressed. The calculated results were compared with the measured gamma dose rates. Good agreement was obtained when the detectors were placed at the middle of the fuel assembly region. The deviations of the calculated dose rates became larger when the measurements were performed at the top or bottom fuel assemblies. In these benchmark studies, the spent nuclear fuel assemblies were all PWR assemblies and had fuel burnup around 25 MWd/kg to 40 MWd/kg. Its cooling time before the measurements was around 1.8 years to 7 years. The used nuclear fuel assembly is usually self-protected while discharged from the core. Its radioactivity decreases and after a few tens of years it may fall down below the current threshold of 100 r/h. Future validation work is necessary in order to better evaluate the numerically calculated gamma dose rates with experiments performed for other types of fuel assemblies and for fuel assemblies with higher burnup and/or longer cooling times.

Validation of Gamma Dose Rate Calculation Methodology using the Morris and Turkey Point Measurements

1. Introduction

The ability to accurately predict the dose rates from the spent nuclear fuel assembly is very important for assessing its self-guard and self-protection properties. Previous studies showed that the direct numerical calculations of the dose rates gave a much lower value [1] than the reference value which was calculated using the gamma buildup factors [2]. In the reference calculations, the gamma dose rate through air were predicted at 1 meter away from PWR spent nuclear fuel assemblies with 33 MWd/kg burnup and 30 years of cooling time. It is understood that these reference values of 1.3-1.52 kR/h are high and conservative with applications intended for shielding design. Using the reference values directly may lead to an overestimated number of years that the spent nuclear fuel assembly can be self-protected. A more accurate evaluation of the dose rates at different cooling time periods is required to determine the proper years that the spent nuclear fuel can be self-guarded. For this application, dose rates with underestimations are on the "conservative" side and are more appropriate.

In this study, the Morris experiments [3] and the Turkey Point experiments [4, 5] are used to assess the numerical procedure used for calculating the dose rates from the discharged spent nuclear fuel assembly. The nuclear fuel assembly becomes radioactive after it is irradiated in the power reactor for a period of time. The nuclear fission produces a significant amount of radioactive fission products. Other fuel assembly structural materials such as cladding, spacers and etc., are also irradiated and some of the materials become radioactive. The overall radioactivity of the fuel assemblies decreases with time due to the decay of many radioactive isotopes. Usually, the neutron-induced dose rates were calculated to be a few orders of magnitude lower than the doses induced by gammas from a spent nuclear fuel assembly [6]. Therefore, the numerical calculations of the dose rates from the spent nuclear fuel assembly focus on calculating dose rates by the gamma emitters.

The experiments to measure the gamma dose rates involve three distinctive steps: the fuel assembly irradiated in the reactor, the fuel assembly cooled and radioactive isotopes decayed, and the fuel assembly transferred to the experimental facility and the dose rates measured. Similarly, the numerical simulations are also performed in three steps. First, fuel burnup analyses are performed to calculate the isotopic compositions of the burned nuclear fuel as well as the irradiated structural materials. Second, the isotopic decay analyses are performed using the calculated material compositions in the first step. The amount of gamma rays and their energy spectra are generated at the end of fuel assembly cooling period. Last, the calculated gamma sources are served as external sources in the photon transport simulations.

The photon fluxes and the conversion to gamma dose rates are calculated by the photon transport codes.

This report summarizes the numerical simulations performed to reproduce the Morris and the Turkey Point experiments. The two experiments were all performed around the 1980s. Many of the experimental details were not well documented or ignored due to the limited numerical simulation power at that time. In section 2, the facilities and the experimental setup of the two experiments will be described as details taken from the literature. The numerical models at different steps for both experiments will be presented in section 3. In particular, sensitivity analyses are performed for the Morris experiments to examine the missing information and different assumptions adopted in calculating the gamma dose rates. In section 4, the numerical results and the experimental data were compared. The methodology to calculate the gamma dose rates of the spent nuclear fuel assembly is evaluated based on the comparisons.

2. Description of the Experimental Setup

A. Morris Experimental Setup

The Morris experiments were a series of gamma dose rate measurements completed in the General Electrical spent fuel storage facility at Morris Operation. The measurements were performed to support the program of developing potential DOE spent nuclear fuel storage at the Morris operation. In these experiments, the gamma dose rates were measured in the vicinity of the discharged spent nuclear fuel bundles. A wide range of fuel types, power levels and burnups were selected in the experiments. Particularly among the 38 fuel bundles selected, four PWR fuel bundles have gamma dose rates measured in the air. Their fuel bundle number was 1A, 2A, 2B and 2D respectively. They were all Westinghouse 14X14 PWR fuel bundles irradiated in the Morris operation unit 1 and 2. Their fuel burnup ranged from 26.4 GWD/MTU to 40.2 GWD/MTU, and the fuel assembly cooling time before measurement ranged from 30 months to 83 months. The main characteristics of the fuel assemblies were listed in Table 1 as well as their fuel burnup and decay histories [3].

In order to measure the gamma dose rates for each individual fuel assembly, the fuel assemblies were moved underwater from the fuel storage to the place where the experimental pit was installed. Figure 1 (a) shows the Morris experimental setup. It was composed of two main parts, with the lower vessel to support the fuel bundle and an upper diving bell. The lower vessel sited on a stainless steel support plate and had a tube welded on top of the plate. The tube was a 9 inch square with internal spacer on the four sides to house the fuel bundles which was a 7.8 inch wide square for PWR fuel. The tube wall was 12 feet tall. It had a slot cut in the upper part and had two adjacent sides removed to form an open corner. The open slot was 7.7 feet down from the top.

Figure 1 (c) shows an X-Y cutoff view of the experimental setup. As shown in the figure, the tube was on one side of the support plate leaving rooms to house the detectors. Lead blocks were added to balance the lower vessel as shown in Figure 1 (a). The whole experimental lower vessel with detectors was submerged under water. To measure the dose rate in the air environment, a “diving bell” which was the main upper part of the experimental setup was equipped to cover both the fuel bundles and the detectors as shown in Figure 1 (a) and 1 (c). Compressed air was added to the bell to repel the water out of the bell for measuring gamma dose rates in the air.

Table 1 Specifications of the Morris fuel bundle 1A, 2A, 2B and 2D and Turkey Point fuel assembly B03 and D04.

Experimental Fuel Bundle	Morris / 1A	Morris / 2A	Morris / 2B	Morris/ 2D	Turkey Point /B03	Turkey Point /D04
Fuel Type (Array)	14 X 14	14 X 14	14 X 14	14 X 14	15 X 15	15 X15
Fuel U235 (%)	3.397	3.865	3.865	3.996	2.55	2.55
Fuel Density (g/cm3)	9.908	10.10	10.10	10.379	10.08	10.08
Cladding Material	Zr-4	SS304	SS304	SS304	Zr-4	Zr-4
Pellet D (Inch.)	0.365	0.3835	0.3835	0.3835	0.365	0.365
Rod D (Inch.)	0.422	0.422	0.422	0.422	0.422	0.422
Pitch (Inch.)	0.556	0.556	0.556	0.556	0.5617	0.5617
Rod length (Inch.)	144	120	120	120	144	144
Fuel Mass (U) / Assembly (Kg)	386	362	362	372	448	448
Power (MW/MTU)	31.8	23.5	23.5	23.5	31.16	31.2
Burnup (GWd/MTU)	40.2	32.4	26.4	30.4	25.77*	26.55
Burnup Time (day)	1264	1379	1123	1294	827	851
Decay Time (month)	48	83	83	30	46	21.6

* This number is calculated using the specified average thermal power per assembly, the fuel mass per assembly and the irradiation full power days from Table 6.1 and Table 6.2. It is slightly different from the value listed in Table 6.2 of the reference [4].

The gamma dose rates were measured by the DMU ion chambers with locations indicated in Figure 1 (b) and 1(c). The fuel assemblies from the Morris operation Unit 1 and 2 used different length of fuel assemblies. In measurements, the top of the fuel assembly was always the reference zero point for the axial detector locations as shown in Table 2. Detectors were movable along three fixed axial lines

A-1, B1 and E-1. The dose rates were measured with detectors at the top, ¾ and middle height of the fuel bundles respectively. Table 2 names each of these detector locations using two numbers, with the arithmetic numbers to represent the detector axial location, and the alphabet “A”, “B” and “E” to represent the fixed line that the detector moved along with. In particular, for axial direction, “0” represents the detector lined up with the top of the fuel assembly. “1” represents the detector at the ¾ height of fuel assembly, and “2” represents the detector at the middle plane of the fuel assembly.

When measuring the gamma dose rates, the detectors were placed at those positions near the open corner of the fuel bundles. The other three corners of the fuel assemblies were covered by the tube. The measured dose rates were found to be significantly different by placing different corners facing to the open slot. These variations were thought mainly due to the variation of the neutron fluxes across the fuel bundles while they were irradiated inside the Morris Operation Units. The final experimental data at each detector location were the average values with different corners facing to the open slot. It was stated that within a confidence limit of 95%, the true gamma exposure rates were within 8% of the average values among the measurements taken from the different corners. Table 3 lists all the averaged gamma dose rates for each detector location and each fuel assembly.

Table 2 Spatial locations of the ion chambers for Morris unit 1 and 2 fuel assemblies.

Detector	Unit 1			Unit 2		
	X (inch)	Y (inch)	Z (inch)	X(inch)	Y (inch)	Z(inch)
0.B	1.6	-1.6	0	1.6	-1.6	0
0.A	7	-7	0	7	-7	0
0.E	-3.9	-10	0	-3.9	-10	0
1.B	1.6	-1.6	-36	1.6	-1.6	-30
1.A	7	-7	-36	7	-7	-30
1.E	-3.9	-10	-36	-3.9	-10	-30
2.B	1.6	-1.6	-72	1.6	-1.6	-60
2.A	7	-7	-72	7	-7	-60
2.E	-3.9	-10	-72	-3.9	-10	-60

Table 3 Measured gamma dose rates for Morris Unit 1 and Unit 2 fuel assemblies.

Detector	Gamma Dose Rate (R/hr)			
	1A	2A	2B	2D
0.B	10.0	3.75	3.0	12.0
0.A	6.50	2.60	2.15	8.00
0.E	5.80	2.63	2.02	9.60

1.B	33.5	16.0	12.5	37.0
1.A	18.0	7.45	6.00	20.3
1.E	18.0	7.30	5.75	20.8
2.B	34.8	16.8	13.5	40.2
2.A	18.1	7.65	6.15	21.9
2.E	18.0	7.51	5.70	22.0

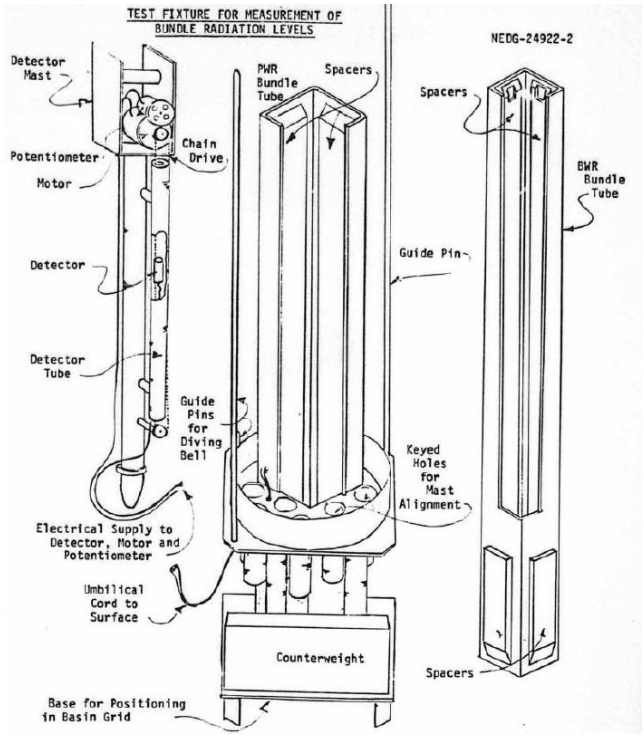

(a)

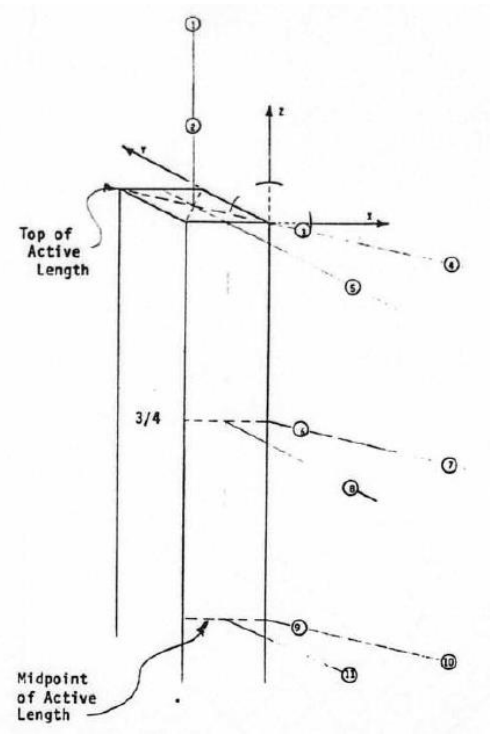

(b)

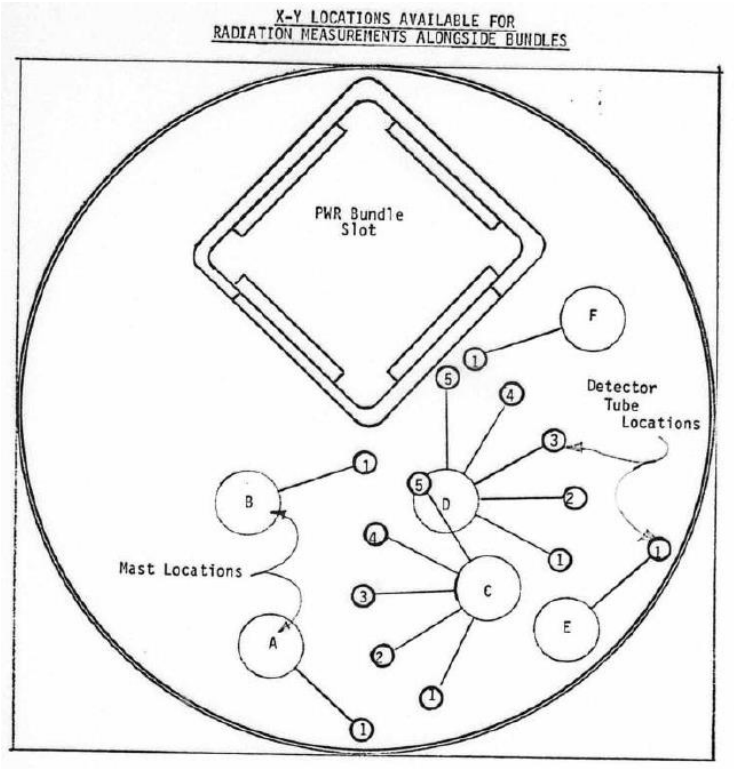

Figure 1. (a) Morris experimental setup. (b) Ion chamber locations relatively to the fuel bundle. (c) X-Y cut view of the experimental setup.

B. **Turkey Point Experimental Setup**

The gamma activities from the spent nuclear fuel assemblies were also measured by a joint effort between the Westinghouse Hanford Company, the Pacific National Laboratory (PNL) and the Battelle-Columbus Laboratories. The fuel assemblies were discharged from the Turkey Point Unit 3 power reactor which was the Westinghouse PWR design. Particularly, two spent fuel assemblies B03 and D04 were examined [4]. They were both Westinghouse 15X15 PWR fuel assemblies. Table 1 also lists the fuel characteristics and the fuel irradiation and decay histories of the two fuel assemblies.

The B03 fuel assembly was irradiated inside the Turkey Point Unit 3 for two cycles with 827 full power days. There were total 1413 days from the fuel assembly loaded into the core till the fuel assembly discharged from the reactor core. The D04 fuel assembly was irradiated in different operation cycles for a total 851 full power days. The time period that D04 stayed inside the core was 1073 days. The total residence time of the fuel assembly in the core included the power reactor down-periods which were not specified in details. The fuel assembly locations inside the core were also not recorded for all the operation cycles. Like the Morris experiments, Table 1 lists the core average fuel burnup for these fuel assemblies which were 25.77 GWd/MTU and 26.55 GWd/MTU respectively. The decay time of the two fuel

assemblies B03 and D04 before measuring the gamma dose rates were 3.8 years and 1.8 years respectively.

The gamma dose rates from the Turkey point fuel assemblies were measured by transferred the fuel assembly to the hot cell at Battelle-Columbus Laboratories. The fuel assemblies were placed on the hot cell table as shown in Figure 2 (a) [4]. The thermoluminescent (TLD) detectors were used in the experiments. Overall there were 315 TLD detectors exposed to the gamma rays for each spent nuclear fuel assembly. Five TLD detectors were packaged together inside a capsule and were wrapped with tissue paper and foil. These capsules were divided into 5 groups. Four of the groups were placed along the fuel assembly to measure the gamma dose rate axial distributions. The last group was placed at the vertical line perpendicular to the fuel assembly to measure the radial gamma dose rate distributions away from the fuel assembly. The axial groups each had 13 capsules and the perpendicular group had 7 capsules. The rest 4 capsules were used to measure the background.

For every detector group, the capsules were placed inside an aluminum tube 1 foot apart from each other. The aluminum tubes were 400 cm long for axial distributions, and it was 213 cm long for vertical distribution. Figure 2(b) shows the positions of those aluminum tubes. Two of the axial tubes were placed inside the fuel assembly and occupied the holes left from the reactor guide tube and instrumentation tube in the fuel assembly. The other two axial tubes were outside the fuel assembly, with one tube sitting directly on the surface of the fuel assembly, and one tube was hanging 1 foot above the assembly flat surface. The vertical tube was on the middle plane of the fuel assembly. Figure 2 (c) shows the reference point used in the measurements. For axial measurements, the reference point is the bottom of the fuel assembly bottom end plug.

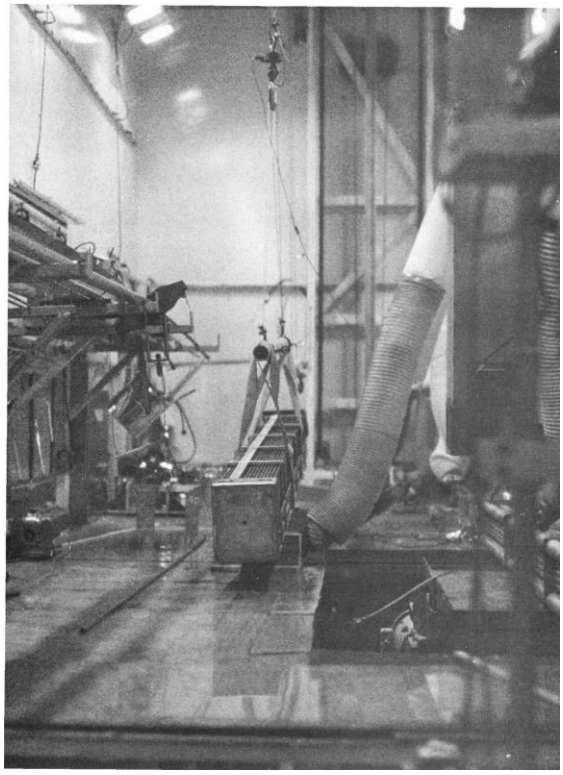

(a)

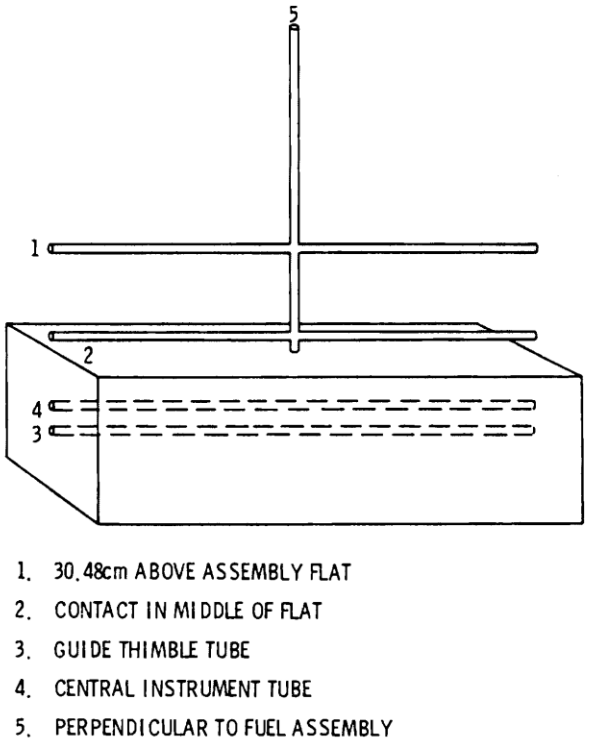

(b)

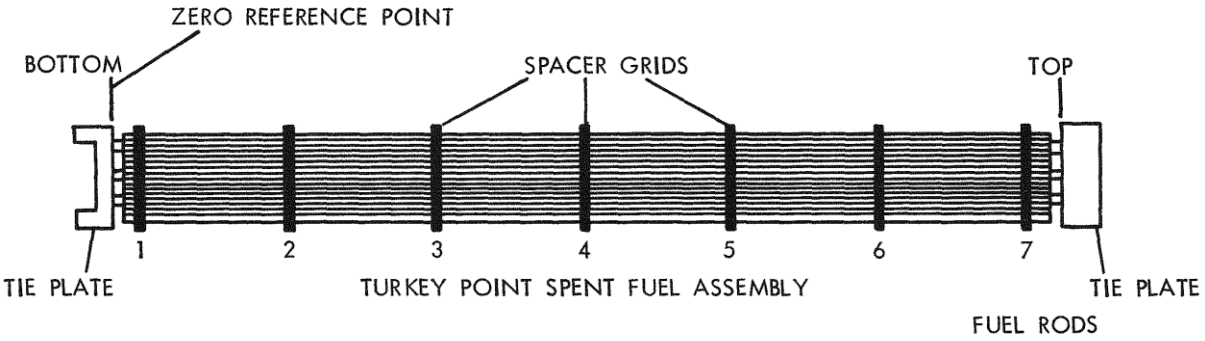

(c)

Figure 2. (a) Fuel assembly B03 in the hot cell for measurements. (b) TLD detector locations relative the fuel assembly. (c) Turkey point fuel assembly reference scheme.

The measured gamma dose rate distributions for fuel assembly B03 are listed in Tables 4 and 6. The experimental data for fuel assembly D04 are only available with detectors located outside the fuel assembly and are listed in Tables 5 and 6. The associated experimental uncertainties are unknown for the fuel assembly D04. In addition, as shown in Table 6, for fuel assembly D04, the actual experiments used 8

capsules to measure the vertical distributions, which is inconsistent to the 7 capsules described previously.

Table 4 Measured axial distributions of the dose rates for Fuel assembly B03.

Detector Location (Distance from reference) (ft)	Instrument Tube		Guide Tube		Assembly Surface		One Foot Away	
	Exposure Rate (kR/h)	1σ (%)	Exposure Rate (kR/h)	1σ (%)	Exposure Rate (kR/h)	1σ (%)	Exposure Rate (kR/h)	1σ (%)
1	38.7	10	175	7	1.32	12	1.74	6
2	133	3	179	4	3.26	3	3.25	4
3	174	5	169	2	22.4	4	6.02	8
4	180	4	167	7	38.1	3	8.39	6
5	181	4	174	4	42.9	3	8.03	9
6	171	4	165	4	56.7	5	11.8	3
7	168	9	172	8	58.8	3	12.3	4
8	168	8	176	5	48.6	5	12.0	5
9	172	8	165	3	63.3	5	12.4	2
10	167	4	125	4	62.3	7	13.1	5
11	163	2	47.7	6	65.7	4	12.9	8
12	127	6	7.18	5	62.6	3	11.7	5
13	62.9	8	1.16	5	57.9	4	10.3	4

Table 5 Measured axial distributions of the dose rates for fuel assembly D04.

Detector Location (Distance from reference) (ft)	Assembly Surface (kR/h)	One Foot Away (kR/h)
1	88.1	7.42
2	89.1	12.1
3	93.0	14.9
4	65.7	16.2
5	92.5	16.2
6	90.0	17.1
7	95.2	16.3
8	93.7	15.8
9	92.7	16.1
10	82.5	15.4
11	54.8	14.2
12	12.9	11.0

13	2.75	7.29

Table 6 Measured radial distributions of the gamma dose rates for the Turkey Point fuel assembly B03 and D04.

Assembly / Dose Rate	Detector Locations (Distance from assembly surface) (ft)								
	0	1	2	3	4	5	6	7	8
B03 (kR/h)	58.8	15.5	7.99	4.62	3.37	2.55	1.90	1.56	---
B03 1σ(%)	3	7	3	4	5	5	6	4	---
D04	63.0	18.6	9.88	6.81	4.91	3.92	3.34	2.85	2.24

3. Numerical Modes and Numerical Simulations

Numerical studies had a similar three-step approach to simulate the Morris experiments. First, the fuel depletion simulation was performed to calculate the discharged fuel compositions from the PWR spent nuclear fuel. Secondly, the radioactive decay simulation was performed to calculate the gamma sources from the radioactive isotope decay at the end of the cooling period. Thirdly, the photon transport simulation was performed to calculate the gamma dose rates at the detector locations using the calculated gamma sources from the second step.

A. Numerical Models and Analysis for the Morris Experiments

The MCODE [7] which couples the MCNP6 [8] neutron transport code and the ORIGEN-2 [9] fuel burnup code was utilized to deplete the fresh fuel bundle. The fuel assemblies used in Morris unit 1 and unit 2 have different fuel lengths, but they share the same lattice design. Figure 3 shows the Monte Carlo model developed for the fuel lattice.

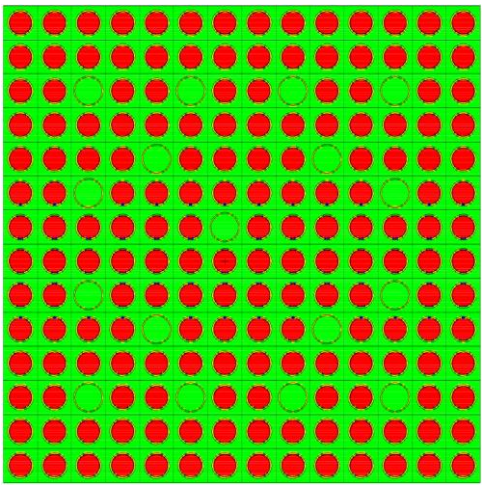

Figure 3. Monte Carlo model of the fuel assemblies for the westinghouse 14X14 fuel assemblies.

The fuel burnup specified for the fuel bundles was the core average burnup. Therefore, the Monte Carlo fuel burnup calculations were performed on the infinite lattice model with reflective boundary conditions applied outside the fuel assembly. The ENDF/B-VII.0 library was used in the Monte Carlo transport calculations, and the ORIGEN-2 library was used for generating the fission products. The MCNP6 code with CINDER90 fuel burnup code imbedded and the SERPENT code [10] were also used to simulate the fuel bundle 1A irradiation for code comparisons. The same ENDF/B-VII.0 data files were used in the transport calculations. In MCNP6 simulations, the tier 3 fission products were selected. Its fission yield libraries were based on the ENDF/B-VI cross section libraries. The SERPENT code used the same cross section libraries for transport calculations and the fission yield libraries are generated from the ENDF/B-VII.0 data files.

Figure 4 compares the calculated reactivity losses by the three codes with fuel burnup days to 1264 days. The reactivity loss ΔKeff calculated by the three codes is very similar to each other with 0.424 by MCODE, 0.425 by MCNP6 and 0.434 by SERPENT. Figure 5 shows the calculated amount of actinides in the fuel bundle at the end of the fuel burnup. Overall, the actinide fuel compositions calculated by MCODE are closer to the compositions obtained from SERPENT. The maximum differences for the U and Pu isotopes are within or around 5% between the MCODE calculation and the SERPENT calculation. The differences for Cm isotopes are slightly larger. About 11% more of Cm242 and 20% less of Cm243 were obtained in the SERPENT code calculations. The MCNP6 fuel burnup calculations predicts more consumption of U235 and more production of Pu239 at the end of the fuel burnup as shown in Figure 5.

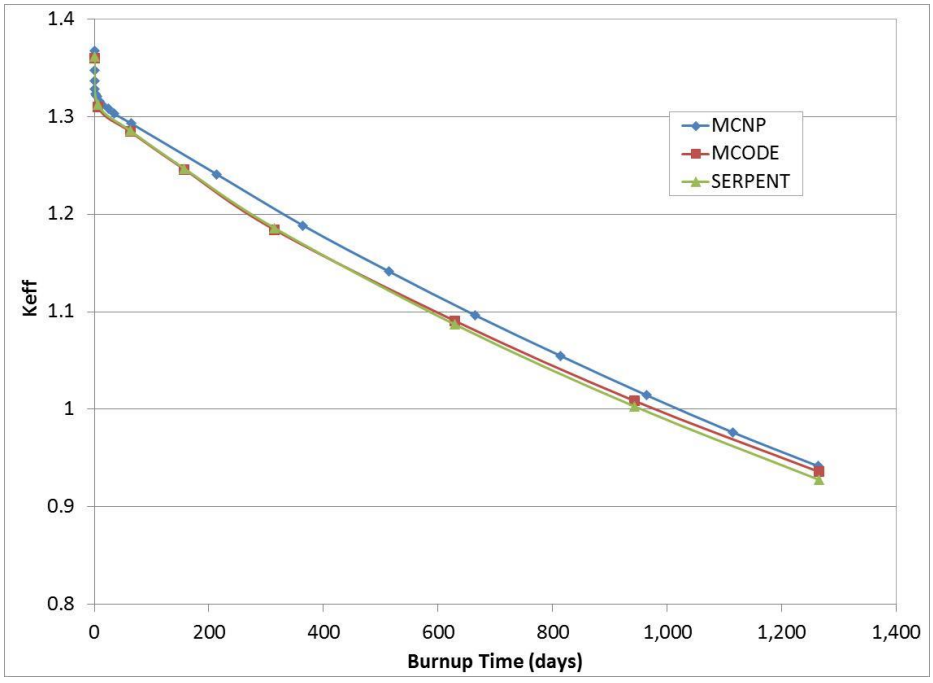

Figure 4. Monte Carlo calculated reactivities in the fuel burnup simulations for the 1A fuel bundle using the MCNP6, MCODE and the SERPENT code respectively.

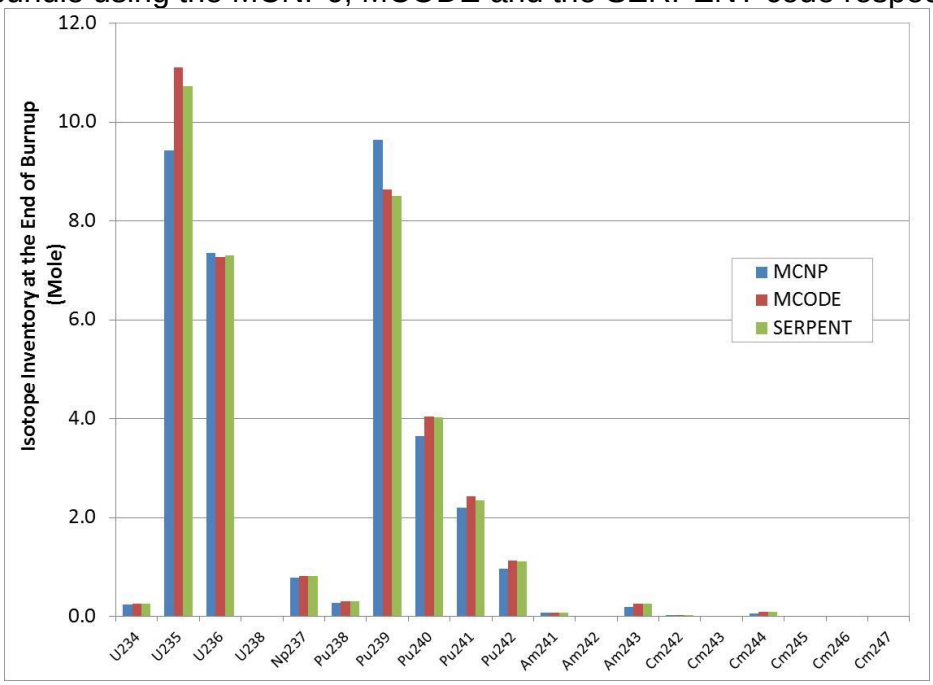

Figure 5. Monte Carlo calculated amount of actinide isotope at the end of the fuel burnup simulations for the 1A fuel bundle using the MCNP6, MCODE and the SERPENT code respectively.

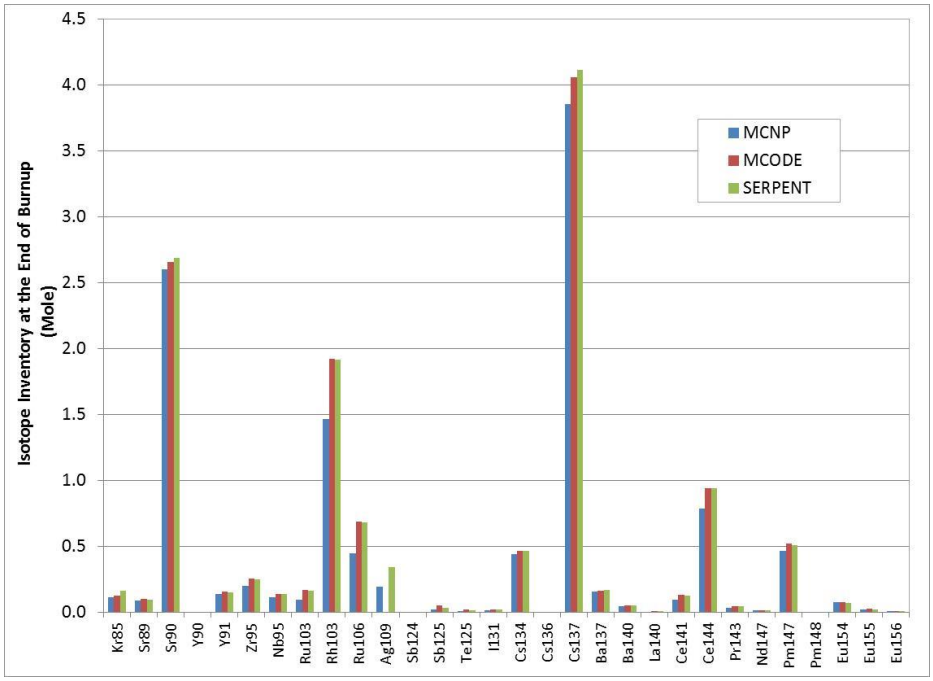

Figure 6. Monte Carlo calculated amount of fission isotopes at the end of the fuel burnup simulations for the 1A fuel bundle using the MCNP6, MCODE and the SERPENT code respectively.

Figure 6 compares the calculated amount of fission products which are important gamma ray source emitters from the three codes. Similarly, the SERPENT and MCODE shows better agreement on the calculated fission product masses. In the MCNP6 fuel burnup analysis, some of the radioactive isotopes at metastable states which are important gamma emitters are not included in the tier 3 fission product library. Therefore, only MCODE was used to perform the fuel burnup analysis for the Morris experiments. The SERPENT code has been used to simulate the Turkey Point experiments as shown in the later section.

The ORIGEN-2 code was used to calculate the gamma source rates of the discharged spent fuel bundle at different cooling stages. The discharged fuel compositions obtained from the fuel depletion calculations were used in the simulations. The gamma ray sources calculated from the code were divided into multiple energy groups. The source rates in each energy group were adjusted to preserve the total amount of gamma source energies released from the fuel assembly. In this benchmark analysis, the default 18 energy group structure of the ORIGEN-2 was used.

Figure 7 compares the multi-energy group gamma sources produced from fission products. The discharged fuel compositions are from the SERPENT burnup simulation or from the MCODE depletion calculations for fuel bundle 1A respectively. The calculated gamma source rates agree with each other very well for both cases at all the energy groups.

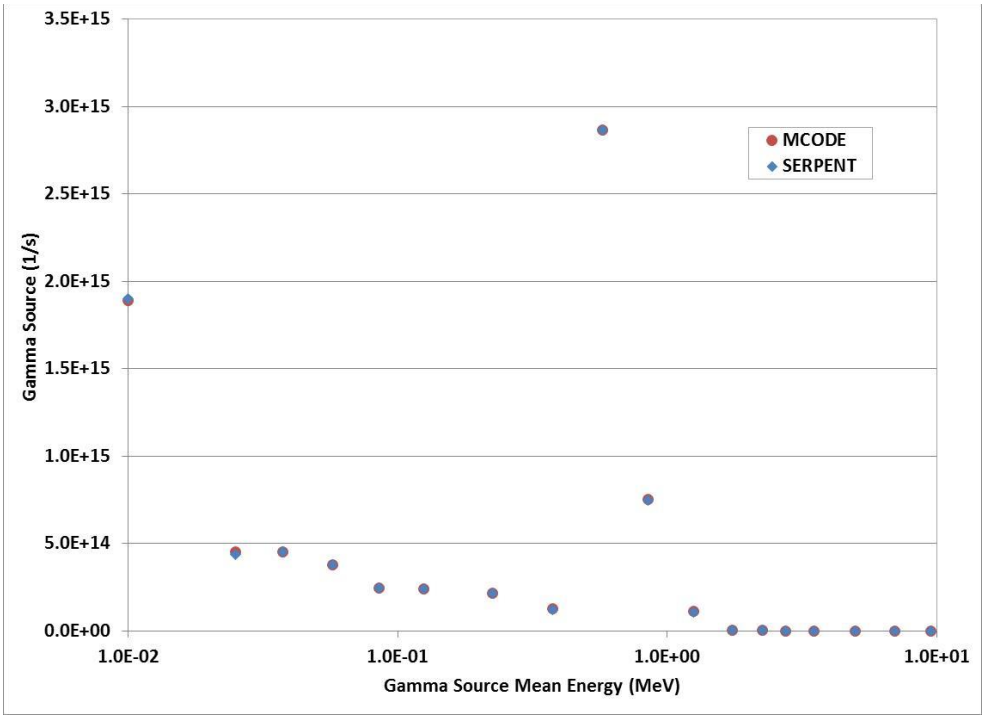

Figure 7. The calculated gamma source energy spectrum of the 1A spent fuel bundle after 4 years of cooling using the SERPENT code and MCODE for fuel burnup analysis.

Table 7 Calculated gamma ray source contributions from the radioisotopes in the Morris discharged fuel assembly 1A at discharge and after 4 years or 30 years of cooling.

Discharge		4 years of cooling		30 years of cooling	
Isotope	Fraction (%)	Isotope	Fraction (%)	Isotope	Fraction (%)
U237	0.697	PU238	0.101	PU238	0.331
SR 89	2.924	AM241	0.123	AM241	1.852
SR 90	0.153	CM244	0.112	CM244	0.167
Y 90	0.941	KR 85	0.328	KR 85	0.246
Y 91	4.308	SR 90	2.598	**SR 90**	5.641
ZR 95	9.359	**Y 90**	15.950	**Y 90**	34.632
NB 95	11.547	**RH106**	15.551	**CS137**	7.333
RU103	7.804	**CS134**	23.701	EU154	1.110
RH106	12.362	CS137	3.317	**BA137M**	48.086
I131	0.800	CE144	1.842	---	---
XE133	0.327	**PR144**	8.857	---	---
CS134	4.754	PM147	0.455	---	---
CS137	0.195	EU154	2.237	---	---
BA140	2.455	SB125	1.636	---	---
LA140	8.337	TE125M	0.356	---	---
CE141	6.289	**BA137M**	21.748	---	---
PR143	0.894	EU155	0.353	---	---
CE144	3.244	---	---	---	---
PR144	15.596	---	---	---	---
ND147	0.997	---	---	---	---
EU154	0.165	---	---	---	---
EU156	1.068	---	---	---	---
RH103M	0.486	---	---	---	---
SB125	0.234	---	---	---	---
BA137M	1.280	---	---	---	---
CS136	0.279	---	---	---	---
PM148M	0.325	---	---	---	---
Total	97.8	Total	97.82	99.3	99.4

The gamma source rates from a spent fuel assembly decreases with longer cooling period. The short lived radioisotopes only contribute to the gamma sources at short cooling times. As an example, for fuel bundle 1A, Table 7 lists the calculated gamma sources originated from each important isotope with contributions larger than 0.1% at different cooling stages. The values in the table are percentage of gamma rays generated from the particular isotopes to the overall gamma source intensities at that cooling stage. Right after the fuel discharged, the Zr-95, Nb-95, Ru-103, Rh-106, LA-140, CE-141, PR-144 isotope contribute more than 71% of gamma sources. After 4 years of cooling, the dominant radioisotopes become Y-90, Rh-106, Cs-134, Pr-144 and Ba-137m which generate about 86% of the total gamma sources. After 30 years of cooling, the dominant radioisotopes for gamma ray sources change to Y-90, Sr-90, Cs-137 and Ba-137m, which contribute more than 95% of the total gamma sources.

While the fuel assembly is irradiated inside the reactor core, the structural materials may also be activated by absorbing neutrons. The grid spacer material in the Morris operation was Inconel 718 which contained a maximum 1% cobalt as part of its impurities. Other structural materials such Zr-4 cladding and SS304 structural material also contained some cobalt impurities. Co-59 is the only stable cobalt isotope in nature which can absorb neutrons and turns to Co-60. Co-60 releases two gamma rays with energies of 1.17 MeV and 1.33 MeV. To calculate the amount of gamma ray sources from the irradiated spacers, Table 8 shows the estimated amount of cobalt mass used in the calculations for all the fuel bundles in the Morris experiments. To simulate the Co-59 impurities irradiated in the core, the neutron cross sections for Co-59 were tallied as shown in Table 9 adopting the neutron flux spectrum inside the guide tubes. The irradiation of Co-59 was then simulated using the ORIGEN-2 code for different fuel bundles.

Table 8 Estimated Co impurities in the Morris fuel assemblies.

Fuel Bundle	1A				2A, 2B, 2D			
	Material	Mass (kg)	Co fr (%)	Co (g)	Material	Mass (kg)	Co fr (%)	Co (g)
Spacer	Inc718	5.9	0.469	27.69	Inc718	5.9	0.469	27.69
Cladding	Zr-4	91.5	0.001	0.92	SS304	89.7	0.08	71.73
Other	SS304	4.6	0.08	3.68	SS304	4.6	0.08	3.68
Total Co (g)	32.29				103.10			

Table 9 MCNP tallied neutron cross sections for Co-59 in the Morris operation at different fuel burnup steps.

Burnup Step (GWd/MTU)	Flux (n/cm2-s)	Tallied Co-59 Cross Sections (barns)			
		(n, gamma)	(n, 2n)	(n, α)	(n, p)
0.2	2.35E+14	5.846	5.69E-5	4.27E-5	3.85E-4
20	2.90E+14	5.409	7.66E-5	4.95E-5	4.23E-4
40.2	3.49E+14	5.416	7.57E-5	5.07E-5	4.34E-4

Figure 8 compares the calculated amount of photon sources produced from the actinides and its daughters, from the fission products and from the Co-60 in the irradiated spacers for the Morris fuel assembly 1A. The gamma ray sources from the spent nuclear fuel assembly are contributed mainly from the decay of the fission products. The gamma rays from other actinide isotopes and the activation products are at least one order of magnitude smaller in all energy groups except in the energy group from 1.0 to 1.5 MeV. The amount of gamma ray sources from the irradiated structural material Co-60 is equally important to the gamma sources released from fission products in this energy group.

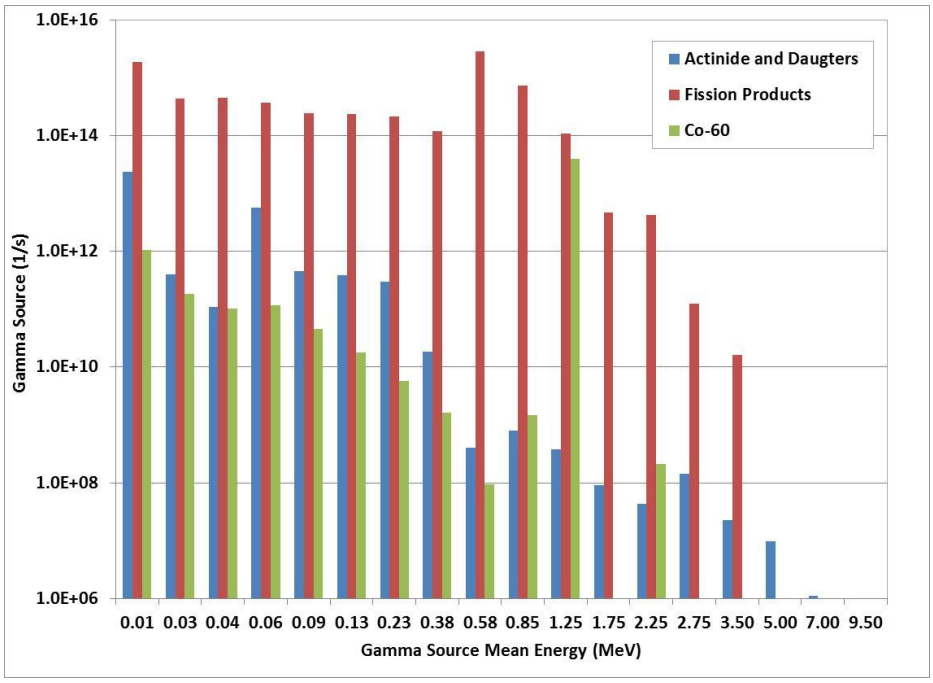

Figure 8. The calculated gamma source energy spectrum from different gamma sources for the 1A spent fuel bundle after 4 years of cooling.

MCNP6 photon transport simulations were performed to calculate the gamma dose rates at the detector locations for the four fuel bundles. The total gamma sources from the ORIGEN-2 decay simulations were specified as external sources in the simulation. The gamma sources were correlated to the radioactive isotopes produced in the fuel pin and in the structural materials. Their actual locations were not accurately determined in numerical simulations. In the Morris experiment, the gamma dose rates were measured outside and away from the fuel assemblies. Thus, in the MCNP6 transport simulation, the gamma sources were assumed to be evenly distributed within the fuel pins in radial direction. Different axial distributions along the fuel pins were tested. The photon fluxes at the detector locations were tallied. The gamma dose rates were then obtained using the flux-to-dose rate conversion factors recommended by the American Nuclear Standard.

Figure 9 shows the MCNP model of the Morris experimental setup with the PWR fuel bundle inside the square tube. The ion chambers used in the experiment were modeled as cylinders which were 0.25 inch in diameter and were 1 inch long. To develop the numerical model, assumptions were made to the geometry parameters which were not specified in the documents. Table 10 lists all these parameters, with different values assigned for each parameter. Sensitivity analyses were performed by comparing the calculate gamma dose rates with different values assigned.

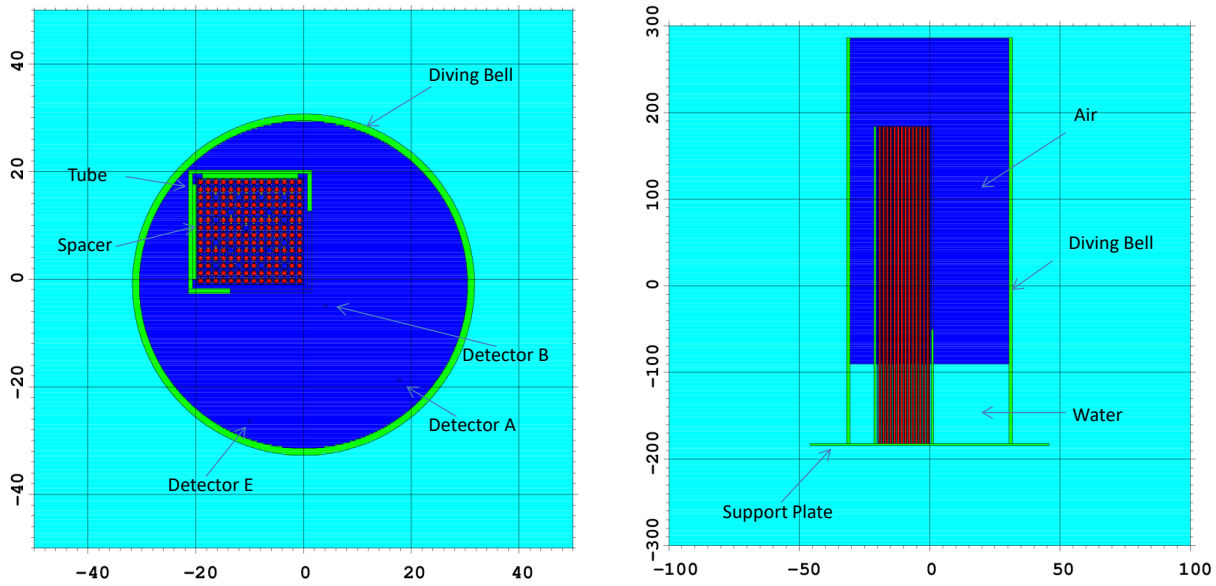

Figure 9. MCNP model of the Morris experimental setup with fuel bundle 1A.

Table 10 MCNP model assumptions and parametric studies for fuel bundle 1A.

Component	Parameter	Values	Sensitivity Analysis
Fuel tube spacer	Thickness	0.3 inch	---
	Width	7 inch	---
Fuel tube slot	Width	(4.5, **6.0**, 8.0) inch	✓
Support plate	Radius	3 feet	---
	Thickness	1 inch	---
Diving bell	Height	(**1.0**, 5.0, 10.0) inch above top detector	✓
	Thickness	0.5 inch	---
	Radius	(**1.0**, 1.25) feet	✓
	Air pressure	(0.5, **1.0**, 2.0) atm	✓
Ion chamber	Radius	0.125 inch	----
	Length	1 inch	----

Water inside the bell	---	(0, **0.25**) height of the tube	✓
Photon source axial distribution	----	(Tuned, uniform, **Wagner**)	✓

In particular, the width of the tube cut slot determines the open space of fuel bundle to the ion chambers and was first examined. The tube slot width varied from 4.5 inch, 6.0 inch to 8.0 inch, respectively. Figure 10 compares the calculate gamma dose rates with the different open width. The photon flux was tallied at the detector locations with its details not simulated. The 1991 updated flux-to-dose conversion factors by the American National Standard were used in the calculations [11].

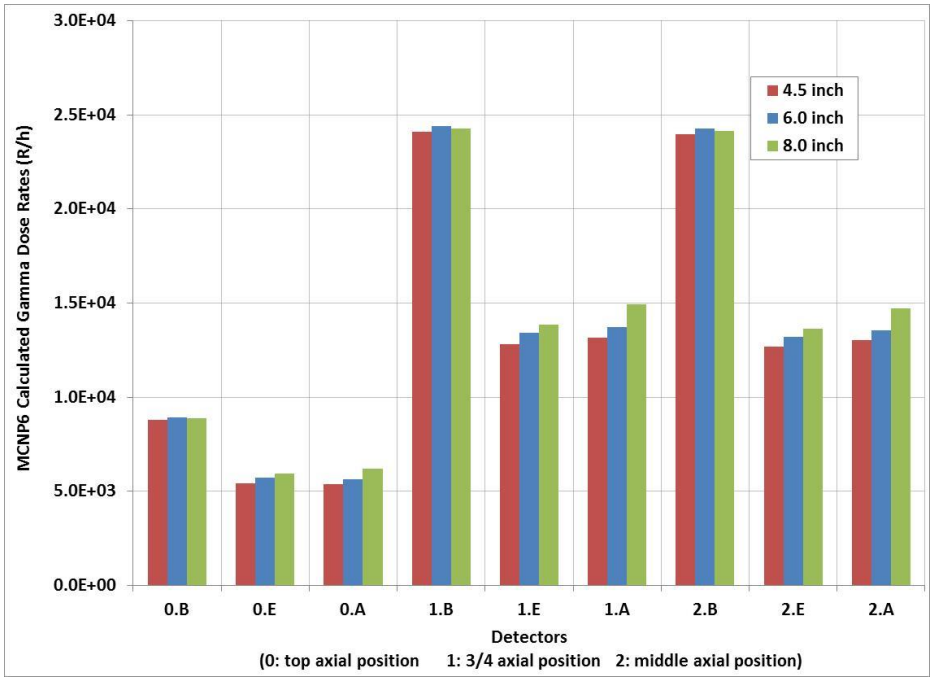

Figure 10. Comparison of the calculated gamma dose rates with different open width of the tube slot for fuel bundle 1A.

As shown in Figure 10, the calculated gamma dose rates are not sensitive to the width of the open slot. The calculated gamma dose rates have no significant differences for all detectors located at the fixed B-1 line closer to the open corner. The dose rates are only slightly increased with wider open slot for detectors at A-1 and E-1 lines. According to Figure 1 (c), the width of the slot can be roughly measured to be about 6 inch based on the relative size in the diagram. Therefore, the width of the slot was selected to be 6 inch in the MCNP model of calculating the gamma dose rates for all the other fuel bundles.

In the Morris experiments, the gamma sources were reflected by the diving bell or were absorbed by the bell. Its impacts to the gamma dose rates were examined by choosing different sizes of the diving bells in the Monte Carlo photon transport

simulations. The diving bell was modeled as a cylinder that sits on the bottom support plate. It covered all the fuel assembly and all the detectors inside the bell. In the actual experiment, as shown in Figure 1 (b), there were two other detectors which were above the fuel tube. Thus, in the MCNP model, to determine the height of the diving bell, an extra maneuverable distance of 1 inch, 5 inch and 10 inch above the detector "**1"** for its operations were assumed respectively. The radius of the diving bell was measured to be around 1 foot according to the diagram in Figure 1 (c). Another case with the radius of 1.25 feet was tested to examine its radial reflection impacts. An independent case without the bell but with water still presented outside the bell was also tested for comparison. Figure 11 shows that the calculated gamma dose rates at all the detector locations are not sensitive to the diving bell geometry. The calculated gamma dose rates all agree with each other for the three cases with different heights, and have only slightly smaller values when the diving bell had larger diameter. The calculated gamma dose rates are only slightly larger with no bell presented, which means the bell absorbed some of the gammas and may also reflect a very small fraction of gammas. Therefore, in the MCNP model, the diving bell was assumed to be a cylinder 1 feet in radius and its top plate 1 cm above the top detector.

To measure the gamma dose rates in the air, the Morris experiments used the compressed air to expel water out of the bell. The MCNP photon transport simulations have also been performed with different air pressures inside the bell. Figure 11 shows the calculated gamma dose rates with different air pressure. The results show that the air pressure have no impact on the gamma dose rates, thus the normal 1 atm pressure was then assumed in MCNP model. In all previous trials, the water was assumed to have been completely pushed out of the bell. A case with water level at ¼ of active fuel length was also tested. As shown in Figure 12, the amount of water left inside the bell has very little impact on the calculated gamma dose rates since the detectors were all far above the water level.

In the MCNP proton transport simulations, the axial distributions of the gamma sources will affect the amount of dose rates calculated for detectors at different heights. In previous trial cases, an axial distribution which was tuned with the intention to improve the calculations at the top detector locations was borrowed. For large PWR reactors, the axial power distribution is flatter than a normal cosine shape, and an axial distribution suggested by Wagner is more realistic to represent the axial fuel pin burnup shape [12]. Thus, a uniform distribution, the previous tuned axial shape and the axial distribution suggested by Wagner were all tested in the Monte Carlo simulations. Figure 13 plots these distributions for comparison. Figure 14 shows the calculated gamma dose rates using the different axial source distributions. Compared with the experimental value, the axial uniform distribution clearly distorts the gamma sources at the end of the fuel bundles (top detector locations). The tuned axial distribution has little impact on the detected dose rates at the middle fuel plane and may improve the results at the top detector locations. But to be more consistent and to apply only reasonable assumptions to the numerical simulations, the Wagner

distributions which represented a type PWR axial burnup shape was used in the Monte Carlo burnup calculations.

In addition, the calculated gamma dose rates are also dependent on the flux-to-dose conversion factors used in the numerical simulations. The most commonly used sets are those by American Nuclear Standard 6.1.1 (ANS-6.1.1-1977) or the updated standard (ANS-6.1.1-1991). The gamma dose rates were calculated using both sets and compared in Figure 15. The gamma dose rates using the 1991 updated set obtained lower dose rates. Therefore, the updated 1991 conversion factor set was more conservative to be used in calculating the gamma dose rates for self-guarding nuclear fuels. It has been used in all the later calculations.

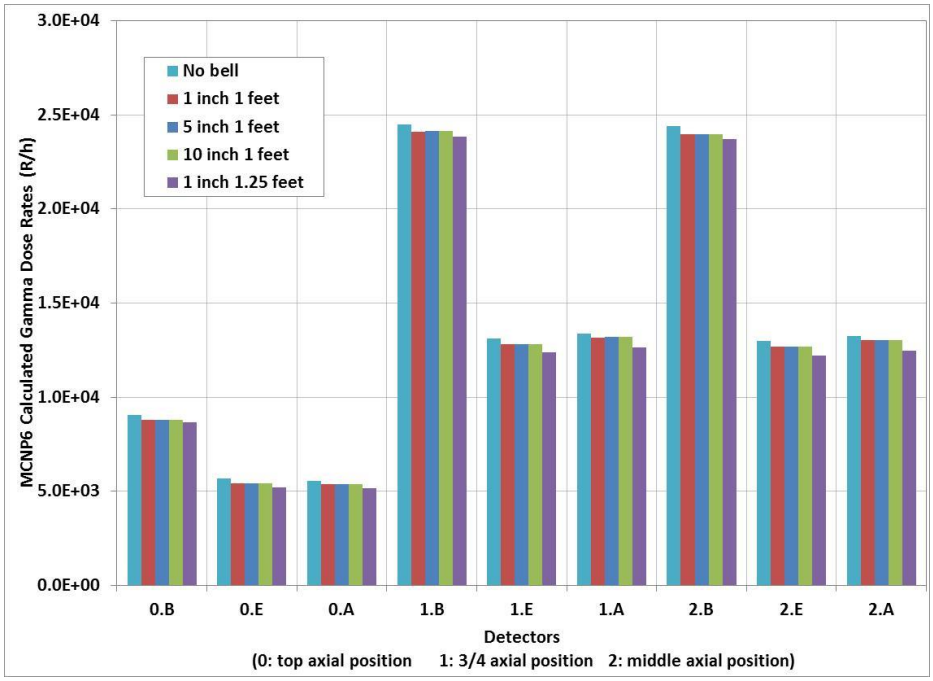

Figure 11. Comparison of the calculated gamma dose rate with different height and diameter of the diving bell for fuel bundle 1A.

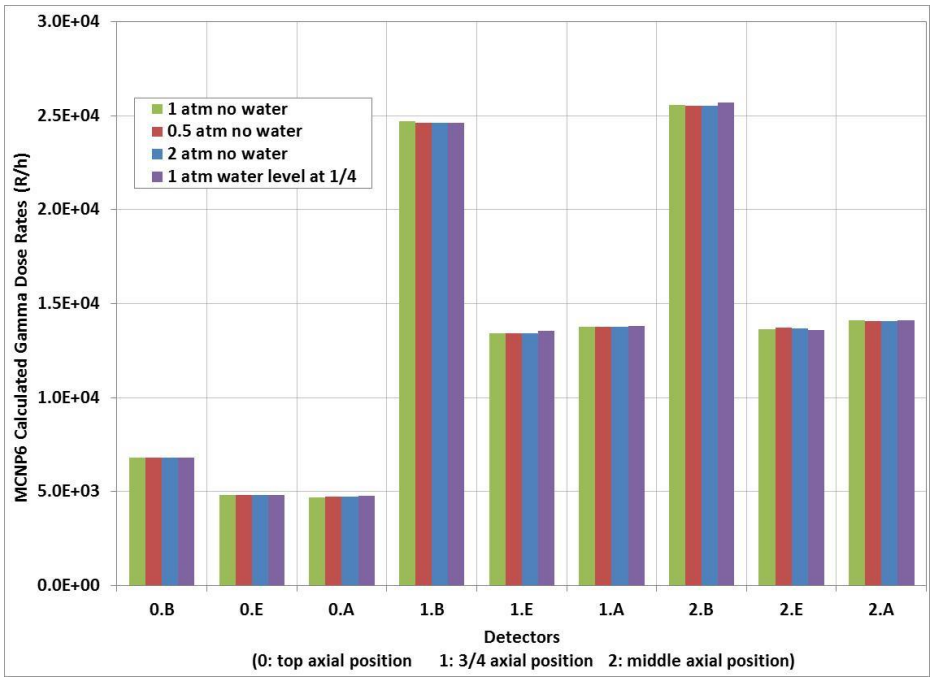

Figure 12. Comparison of the calculated gamma dose rate with different air pressure and water level inside the diving bell for fuel bundle 1A.

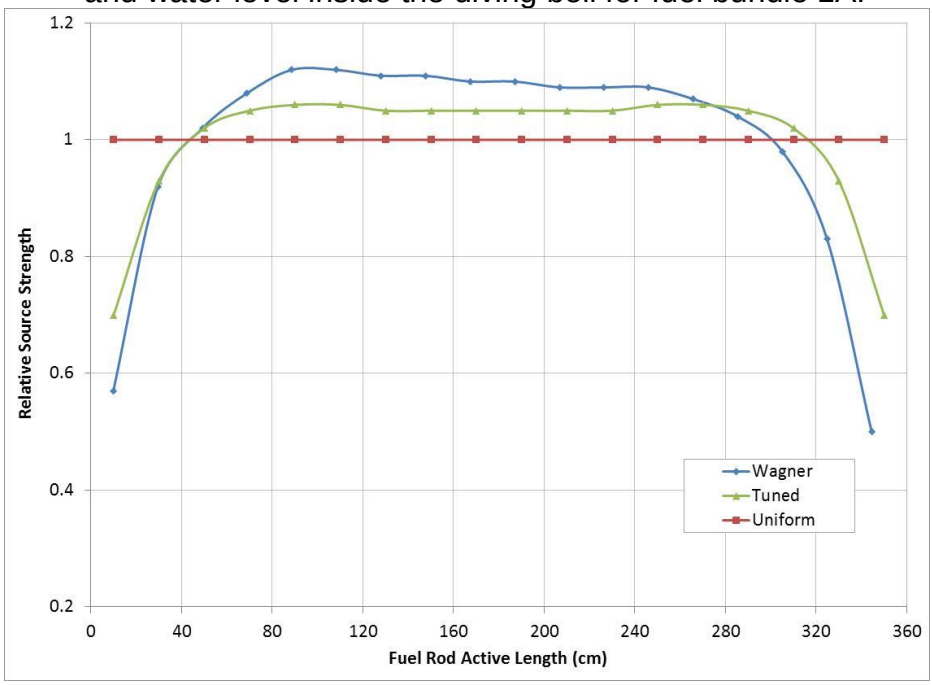

Figure 13. Axial gamma source distributions tested in the Monte Carlo transport simulations for fuel bundle 1A.

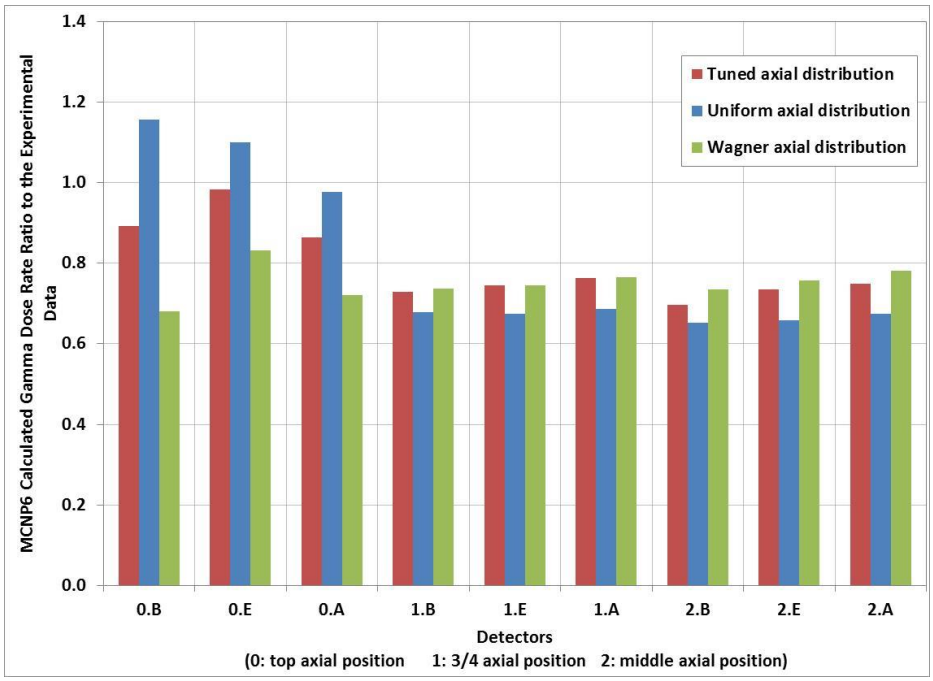

Figure 14. Comparison of the calculated gamma dose rate ratios (MCNP model value vs experiment data) with the three aixal fuel burnup distributions for fuel bundle 1A.

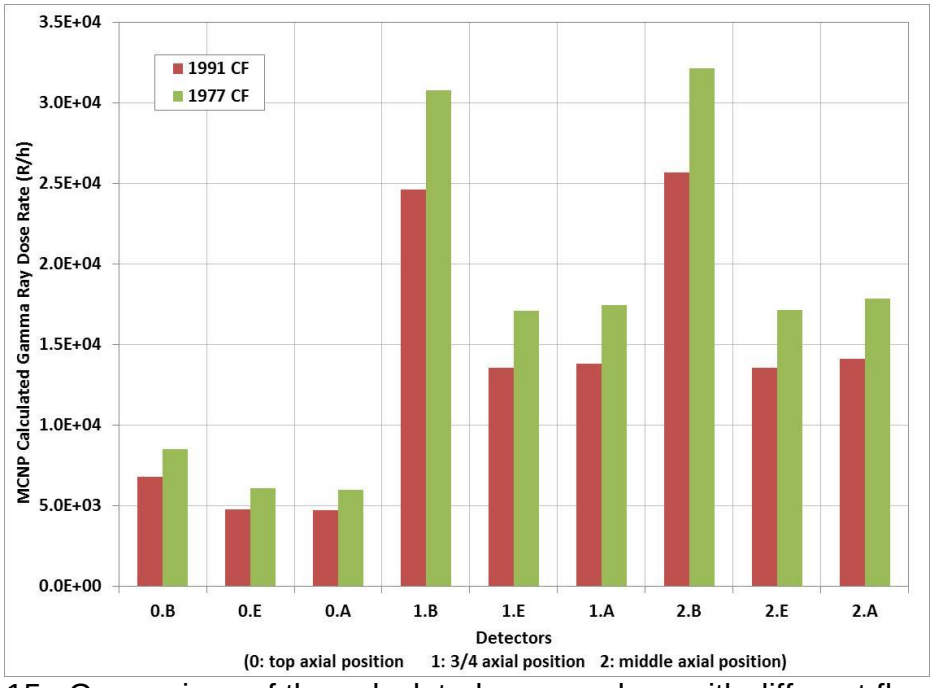

Figure 15. Comparison of the calculated gamma dose with different flux-to-dose conversion factors for fuel bundle 1A.

B. **Numerical Models and Analysis for the Turkey Point Experiments**

The SERPENT code has been used to simulate the depletion of the fuel assemblies B03 and D04 in the Turkey Point experiments. The two assemblies were almost the same except they have different irradiation histories and decay times. Figure 16 shows the Monte Carlo model of the 15X15 Westinghouse PWR fuel assembly used in the analysis.

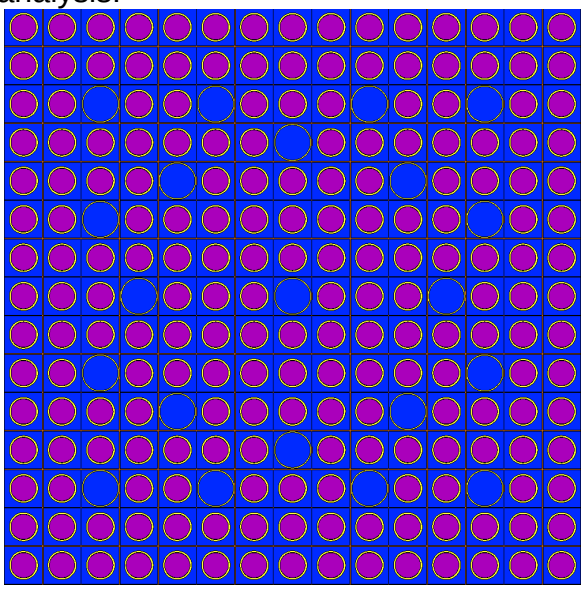

Figure 16. Monte Carlo model of the fuel assemblies for the westinghouse 15X15 fuel assemblies.

Similar to the numerical simulations for the Morris experiments, the fuel burnup analyses were performed with an infinite lattice to match the average core burnup specified in the experiments. Reflective boundaries have been assigned in the radial directions. Different from previous cases, the fuel springs, the fuel spacers, as well as the end caps of each fuel pins have been modeled specifically. Below and on top of the fuel assembly, about one meter water was assumed. The neutrons leaking out of the water boundary were assumed to be lost.

To model the impurities inside the fuel assemblies, particularly cobalt, the total weight of each Inconel 718 fuel spacer was assumed to be 675 grams. The model assumed that each of the spacers was 1.5 inch tall. The spacer axial positions were read from the Westinghouse 15 X15 fuel assembly diagram in Figure 2 of Weihermiller's report [13]. Its cross sectional area was calculated to be 21.63 cm^2 to preserve its total mass. In the B03 and D04 fuel assemblies, the fuel spring material was also Inconel. The SERPENT model assumed that the spring used the same Inconel 718 material as the spacer. It was smeared with a reduced mass density of 4.555 g/cm^3 to preserve its total mass inside the spring zone. The total weight of the spring was assumed to be 11.34 Kg (25 lb). In our numerical model, the Inconel 718 material composition was read from McConn's report [14], with about 0.91% weight percent of Co-59 included. The B03 and D04 fuel pins used Zr-4 as cladding material which has a much lower concentration of Co-59 impurities. Thus, its impurities have been ignored in the model.

Monte Carlo fuel burnup analyses were performed to simulate the fuel depletion and the irradiation of Co-59 impurities. Separate burnup regions were assigned for the seven spacers and for the spring, respectively. The Monte Carlo fuel burnup calculations were performed continuously with no reactor outage time simulated.

Figure 17 plots the calculated reactivity drop of the fuel assembly for both assemblies up to its specified fuel burnup. Overall, the B03 fuel assembly lost about 2879 pcm of reactivity after 25.8 GWd/MT burnup, and D04 lost about 2928 pcm of reactivity after 26.6 GWd/MT burnup. Table 11 shows the amount of Co-59 and Co-60 impurities before and after irradiation. More Co-59 in the spacers are transmuted because the spacers are located at the higher neutron flux zone compared to the springs. The total amount of Co-60 generated in the spacers is about 3 times the Co-60 generated in the springs for both B03 and D04 fuel assemblies.

Table 11 Monte Carlo Calculated Co-59 transmutation and Co-60 production in the Turkey point fuel assembly B03 and D04.

Fuel Assembly	B03		D04	
	Spacer	Spring	Spacer	Spring
Co-59 initial mass (g)	43.0	103.2	43.0	103.2
Co-59 mass at discharge (g)	39.7	102.2	39.6	102.2
Co-60 mass at discharge (g)	2.96	0.86	3.05	0.90

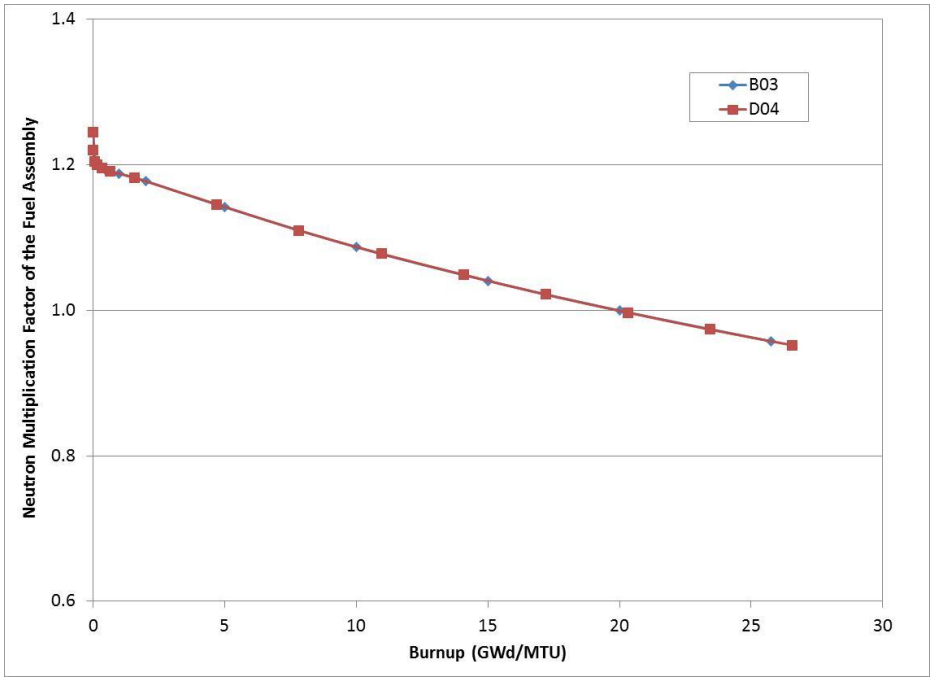

Figure 17. SERPENT calculated reactivity losses during the fuel burnup for the Turkey Point fuel assembly B03 and D04.

The ORIGEN-S code is the most recent version of the ORIGEN code [15]. It has major upgrades for the nuclear libraries compared to the ORIGEN-2 code. The photon emission yields have been updated using the most recent line-energy yields

in the Evaluated Nuclear Structure Data File (ENSDF). To calculate the multi-group gamma source rates from the spent fuel assemblies B03 and D04, the decay of the radioactive isotopes has been simulated using the ORIGEN-S code.

The gamma ray sources released from the spent fuel fission products, from the irradiated spacers and from the irradiated spring were all calculated separately using the material compositions generated from the SERPENT code. The default 18 energy groups in the ORIGEN-S code, as listed in Table 12, were used to tally the gamma sources.

Table 12 Default 18-energy group structures for gamma spectra in ORIGEN-S code.

Group	Upper Boundary Energy (MeV)	Group	Upper Boundary Energy (MeV)	Group	Upper Boundary Energy (MeV)
1	0.02	7	0.25	13	2.60
2	0.035	8	0.40	14	3.00
3	0.05	9	0.90	15	3.50
4	0.075	10	1.35	16	4.00
5	0.125	11	1.80	17	4.50
6	0.175	12	2.20	18	5.00

Figure 18 shows the calculated gamma ray sources from the fuel zone, from the spacers and from the spring respectively. Overall, the major gamma sources are contributed by the decay of fission products. The Co-60 gamma rays, particularly those released from the irradiated spacers, are one of the main contributors to the overall gamma sources with energy around 0.9 MeV to 1.35 MeV. The total gamma source intensity obtained from the calculations is 4.74E+15 /s from the B03 fuel assembly after about 3.8 years of decay, and is 1.36E+16 /s from the D04 fuel assembly after about 1.8 years of decay.

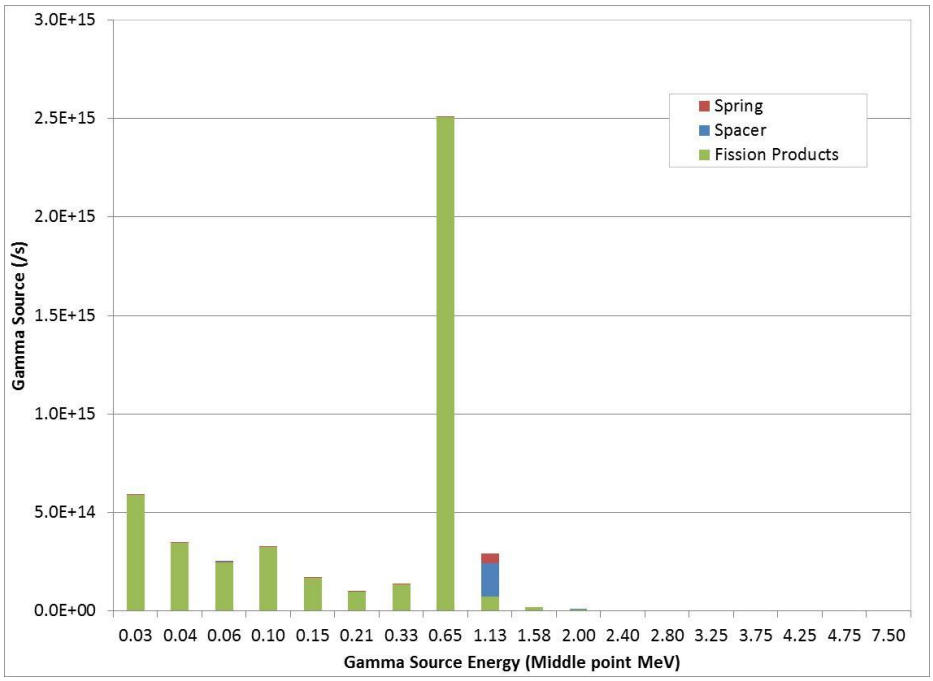

Figure 18. Calculated gamma source spectra from the decay of fission products, decay of Co-60 in the spring and spacer for Turkey Point fuel assembly B03.

In the experiment, the gamma dose rates were measured in the hot cell. The fuel assemblies were modeled to be sitting on the 25 cm thick concrete floor as shown in Figure 19. The other concrete walls of the hot cell were 2 meters away from the fuel assembly. The TLD detectors were modeled as LiF cylinders which have the same radius as the fuel pellet and height of 4.6 cm. The aluminum tube holding the TLD detectors were modeled with its inner and outer radius the same as the fuel pin cladding. To put all the aluminum tubes within one geometry model, the vertical aluminum tube was assumed to be shifted slightly from the center to avoid overlapping with the two horizontal aluminum tubes as shown in Figure 19 (b).

The gamma sources calculated from the ORIGEN-S have been used as external sources to support the MCNP photon transport simulations. For both fuel assemblies, three separate transport simulations were performed using the gamma sources from the fuel, the spacer and the spring, respectively. The gamma dose rates at each detector location were calculated separately. The sum of the three calculated gamma dose rates was then compared with the experimental data.

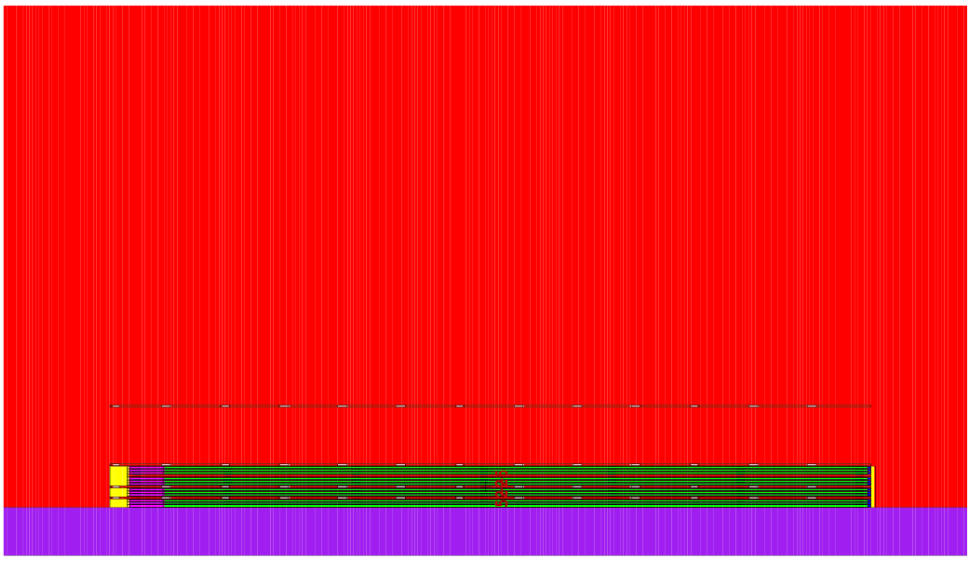

(a)

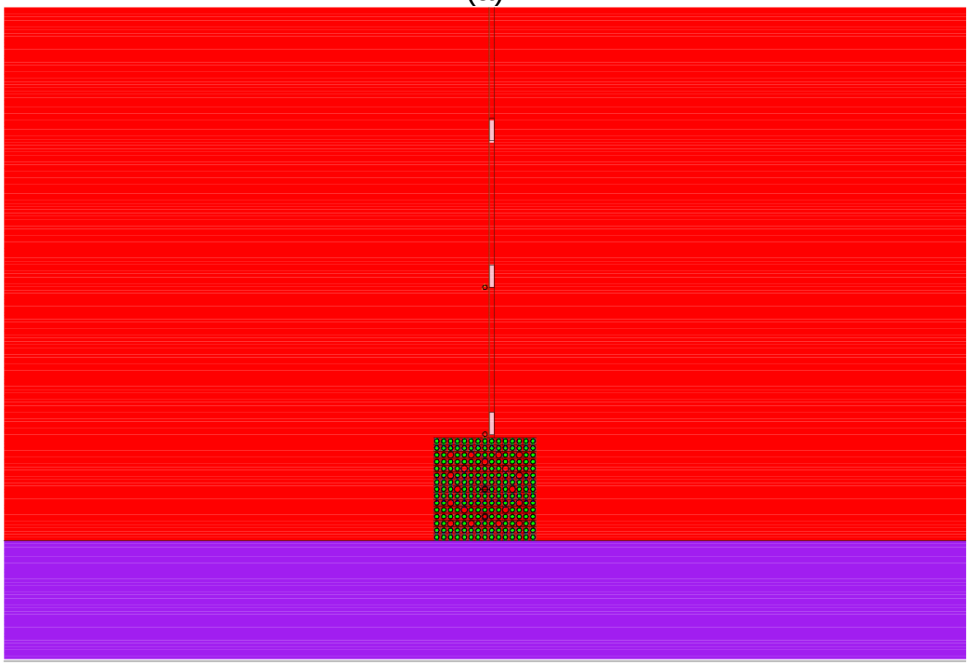

(b)

Figure 19. MCNP model of the Turkey Point experiments to (a) review graph showing the horizontal aluminum tube and the the detectors (b) review graph showing the vertical aluminum tube and the detectors.

For this study, to perform the photon transport simulations, the gamma sources released from the fission products were assumed to be uniformly distributed in each fuel pin radially and distributed axially according to the Wagner fuel burnup distribution. Similarly, the gamma sources released from the spacers were also assumed to be uniform within each of the spacers. Its relative total source strength among the seven spacers was calculated using the Wagner axial distributions based on its axial location. The gamma sources released from Co-60 in the spring zone were assumed to be evenly distributed inside the spring zone for simplicity.

4. Results Comparison and Experimental Validations

A. Morris Experiments Simulation Results and Comparison

The selected geometrical parameters of the Monte Carlo model used to simulate the Morris experiment setup have been put in bold fonts shown in Table 9. Table 13 lists the calculated gamma dose rates for all four fuel bundles at each detector location. Figure 20 plots the gamma dose rate ratios of the calculated values to the measured values.

Table 13 MCNP calculated gamma dose rates for the four fuel bundles in the Morris experiments.

Detectors	1A		2A		2B		2D	
	kR/h	C/E	kR/h	C/E	kR/h	C/E	kR/h	C/E
0.B	6.81	0.68	3.16	0.84	2.56	0.85	7.22	0.60
0.E	4.83	0.83	2.42	0.92	1.95	0.89	5.55	0.58
0.A	4.69	0.72	2.35	0.90	1.90	0.88	5.35	0.67
average	---	0.74	---	0.89	---	0.87	---	0.62
1.B	24.7	0.74	13.6	0.85	11.0	0.88	31.1	0.84
1.E	13.4	0.75	7.13	0.98	5.76	1.00	16.4	0.79
1.A	13.8	0.77	7.41	0.99	5.99	1.00	16.9	0.83
average	---	0.75	---	0.94	---	0.96	---	0.82
2.B	25.6	0.73	13.9	0.83	11.2	0.83	31.7	0.79
2.A	13.6	0.76	6.86	0.91	5.54	0.97	15.7	0.71
2.E	14.1	0.78	7.43	0.97	6.01	0.98	17.0	0.78
average	---	0.76	---	0.90	---	0.93	---	0.76

Overall, compared with the measured gamma dose rates, the numerical calculations do not overestimate the measured gamma dose rates. The calculated gamma dose rates agree better with the experimental values for those from detectors at the ¾ height of the fuel assembly or at the axial mid-plane than for those from detectors located at the top of the fuel assemblies. The calculated gamma dose rates are always closer to the experimental values for fuel assemblies 2A and 2B than for fuel assemblies 1A and 2D. In particular, for fuel assembly 2A and 2B, the average gamma dose rates among the three fixed lines at each axial location are about ~10% underestimating the experiment values. For fuel assembly 1A, the averaged dose rates at all three axial locations are consistent and about 25% lower than the experimental values. For fuel assembly 2D, the calculated gamma dose rates are about 40% lower at the top detector location, and about 25% lower at the middle

plane, and about 18% less at the ¾ height position. The fuel assemblies 2A and 2B have similar characteristics. They were also irradiated in the core for similar amount of time, have similar amount of fuel burnup, and are waited all about 83 months before the measurements. However, the fuel assembly 1A and 2D have different fuel characteristics. More importantly, the decay time for fuel assembly 1A and 2D is much shorter. As shown in Table 7, the dominant gamma ray emitters from the spent fuel assemblies change along the fuel assembly cooling time as some of radioisotopes decay quicker than others. Further research work with experimental data covered with all periods of decay time is required to evaluate the different discrepancies from the experimental data shown in this analysis.

The calculated gamma dose rates at the top detector locations are strongly dependent on the axial gamma source distributions used in the simulations. The Wagner axial distribution is an assumption of the fission products distributions in the fuel bundles. Fission gases like Kr85 easily migrate to the gas plenum region and are also strong gamma emitters. Numerical simulations have ignored the fission gas plenum or its migration or release during the fuel irradiation and cooling period. Bearing these limitations, the calculated gamma dose rates of the Morris experiments still reasonably agree with the experimental data. The numerically calculated gamma dose rates from the spent nuclear fuel are always on the conservative side for the purpose of evaluating its abilities of self-guarding and self-defending.

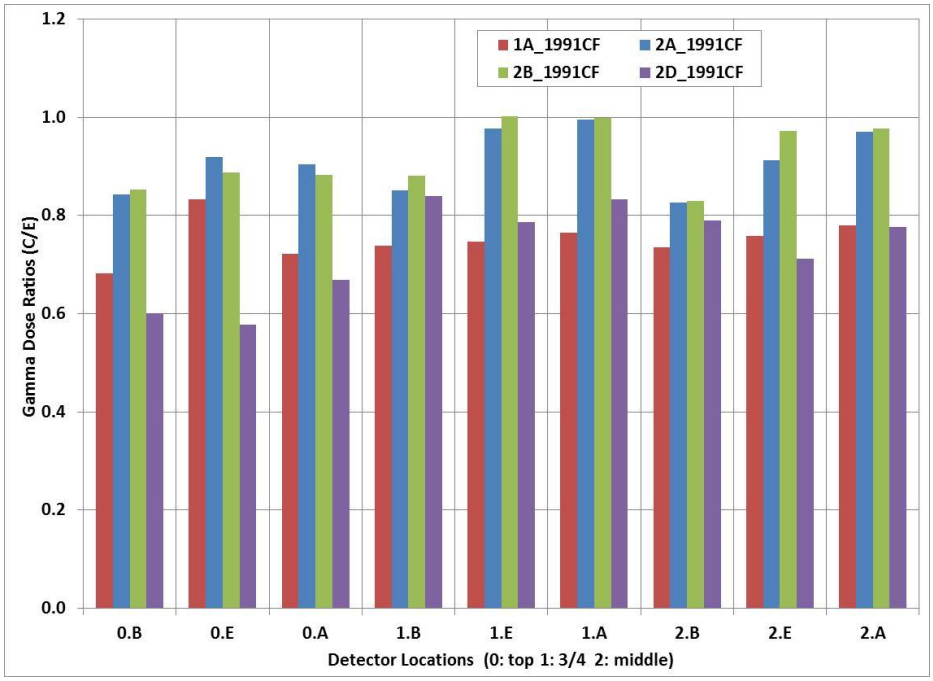

Figure 20 Comparison of the calculated gamma dose rate ratios to the measured values for fuel bundle 1A, 2A, 2B and 2D in the Morris experiments.

B. **Turkey Point Experiments Simulation Results and Comparison**

To simulate the Turkey Point experiments, the gamma dose rates were calculated using each gamma source from the fission fuel zone, from the spacer, and from the spring zone respectively. The total gamma dose rates at each detector location were the sum of three components (assuming that they are additive). The same numerical models, except for different burnup times and fuel assembly cooling times, were used for simulating both fuel assemblies B03 and D04. Table 14 to 16 lists the calculated total gamma dose rates for the two fuel assemblies. Figures 21 to 28 compare the calculated gamma dose rates with the experimental values. The data are grouped according to the detectors inside each aluminum tube.

Table 14 Calculated axial gamma dose rates for fuel assembly B03.

Distance from reference (ft)	Instrument Tube		Guide Tube		Assembly Surface		One Foot Away	
	kR/h	C/E	kR/h	C/E	kR/h	C/E	kR/h	C/E
1	57.76	1.49	54.64	0.31	27.07	20.51	5.11	2.94
2	79.94	0.60	76.19	0.43	38.37	11.77	7.21	2.22
3	70.91	0.41	67.42	0.40	33.42	1.49	7.65	1.27
4	74.45	0.41	70.50	0.42	35.43	0.93	8.10	0.96
5	71.58	0.40	67.69	0.39	33.74	0.79	8.02	1.00
6	70.44	0.41	67.26	0.41	33.41	0.59	8.01	0.68
7	72.19	0.43	68.57	0.40	34.38	0.58	8.03	0.65
8	69.35	0.41	65.88	0.37	32.75	0.67	7.88	0.66
9	81.30	0.47	77.50	0.47	39.37	0.62	7.80	0.63
10	62.64	0.38	59.18	0.47	29.45	0.47	7.00	0.53
11	125.1	0.77	120.7	2.53	48.40	0.74	6.33	0.49
12	91.04	0.72	84.66	11.79	42.99	0.69	5.60	0.48
13	3.64	0.06	3.26	2.81	2.77	0.05	3.69	0.36

Table 15 Calculated radial gamma dose rates for the fuel assembly B03 and D04.

Assembly Dose Rates		Detector Locations (Distance from assembly surface) (ft)								
		0	1	2	3	4	5	6	7	8
B03	kR/h	40.35	7.10	3.56	2.28	1.63	1.16	0.87	0.62	---
	C/E	0.69	0.46	0.45	0.49	0.48	0.45	0.46	0.40	---
D04	kR/h	80.14	15.24	7.62	4.87	3.47	2.43	1.75	1.25	---

	C/E	1.27	0.82	0.77	0.72	0.71	0.62	0.52	0.44	---

Table 16 Calculated axial gamma dose rates for fuel assembly D04.

Distance from reference (ft)	Instrument Tube		Guide Tube		Assembly Surface		One Foot Away	
	kR/h	C/E	kR/h	C/E	kR/h	C/E	kR/h	C/E
1	131.72	---	124.60	---	62.12	0.71	11.19	1.51
2	169.89	---	161.99	---	81.25	0.91	15.52	1.28
3	162.20	---	153.84	---	76.49	0.82	16.56	1.11
4	167.47	---	157.67	---	78.84	1.20	17.50	1.08
5	163.13	---	154.02	---	76.73	0.83	17.40	1.07
6	160.38	---	153.05	---	75.95	0.84	17.24	1.01
7	161.85	---	153.75	---	77.18	0.81	17.34	1.06
8	158.57	---	150.04	---	75.04	0.80	17.03	1.08
9	173.59	---	165.28	---	83.93	0.91	16.59	1.03
10	143.41	---	135.35	---	67.70	0.82	14.86	0.96
11	220.19	---	210.77	---	88.81	1.62	12.79	0.90
12	91.04	---	84.66	---	42.99	6.35	5.60	0.92
13	3.64	---	3.26	---	2.77	1.44	3.69	0.86

Overall, the calculated gamma dose rates show significant differences from the measured experimental data. For detectors inside the fuel assembly B03 as shown in Figure 21 and 22, the calculated gamma dose rates are less than half of the measured dose rates at most of the detector locations.

The calculated gamma dose rates have different axial shapes from the experimental data along the fuel assembly. In particular, the calculated gamma dose rates have peak values at 11 feet from the reference point, where the second spacer from the top of the fuel assembly is located just nearby. Table 17 breaks down the calculated gamma dose rates into three components at this axial detector location. It shows that the peak is due to the increased contribution from the spacer. The peak is consistently shown in all calculated axial distributions in Figures 21, 22, and 23.

The calculated gamma dose rates for the detectors inside the instrument tube, the guide tube or the tube contacting surfaces have very similar axial shapes along the fuel assembly. The experimental data only have a similar axial shape as the numerical calculations for detectors inside the guide tube as shown in Figure 22. The experimental data axial shape is completely different from the calculated axial shape for detectors inside the instrument tube as shown in Figure 21, or for detectors one foot above the fuel assembly as shown in Figure 24. Figure 23 shows the experimental dataset has a reversed shape from the numerical calculations for

detectors resting on the fuel assembly surfaces. The inconsistency of the axial shape distributions leads to serious questioning of the accuracy of the experimental data set.

Table 17 Calculated the gamma dose rates from the gamma ray sources for detectors located about 11 feet from the reference point in the instrument tube, guide tube and tube on the assembly surface respectively.

Calculated gamma dose rates (kR/h)	From fuels			From spring			From spacers		
	11	12	13	11	12	13	11	12	13
Detector in instrument tube	50.0	57.0	0.15	0.068	33.3	3.06	75.0	0.74	0.44
Detector in guide tube	47.3	53.8	0.13	0.075	30.2	2.73	73.4	0.71	0.4
Detector on assembly surface	23.5	25.2	0.19	0.070	17.3	2.26	24.9	0.51	0.31

Figures 23 and 24 include the calculated gamma dose rates contributed by the three types of gamma ray sources. It shows that the Co-60 gamma lines contribute significantly to the gamma dose rates when the detectors are very close to the Co-60 source. Its contribution decreases quickly when the detector is away from the spacers as shown in both figures. The spring is at the top end of the fuel assembly. The activation product Co-60 only impacts the gamma dose rates measured at the last two or three detectors near the spring zone as shown in the two previous figures.

In addition, Figure 25 compares the gamma dose rates at vertical locations perpendicular to the fuel assembly. The calculated gamma dose rates at these positions are all about 40% to 50% of the measured gamma dose rates.

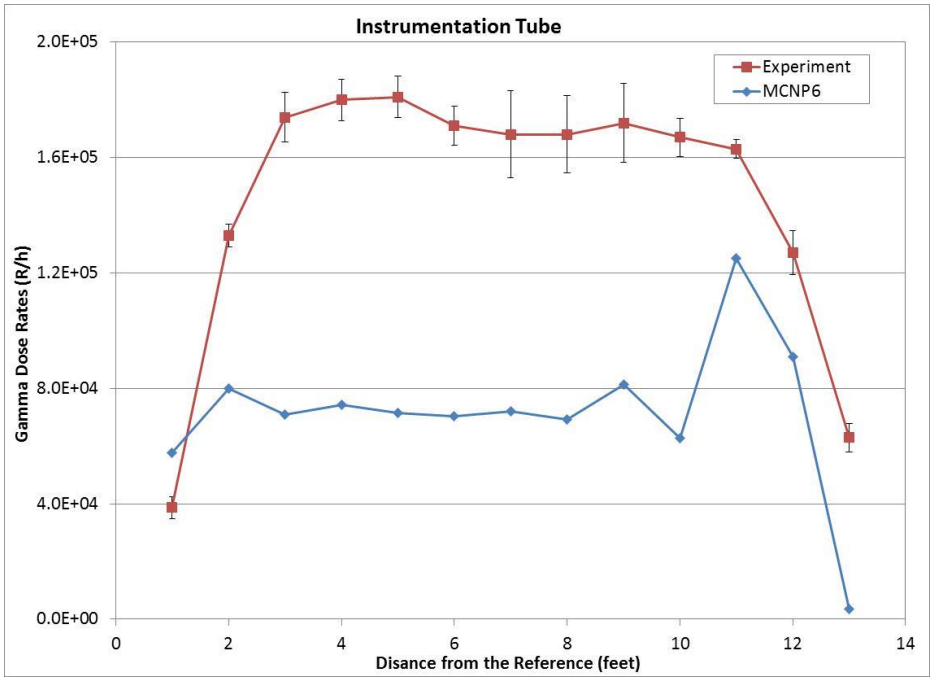

Figure 21 Comparison of the calculated gamma dose rates and the measured values for detectors inside the instrumentation tube of the fuel assembly B03.

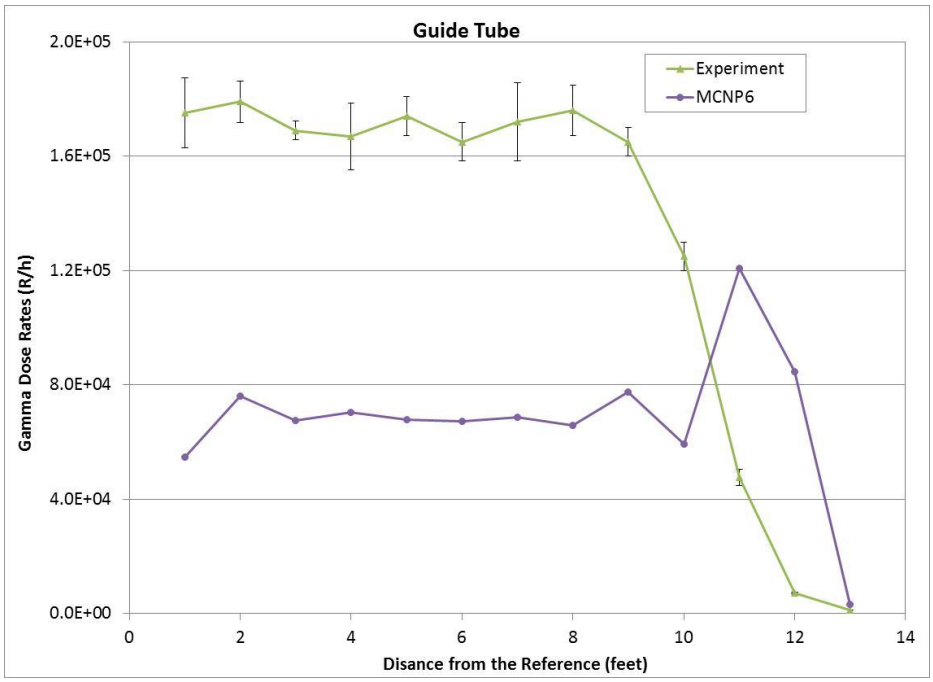

Figure 22 Comparison of the calculated gamma dose rates and the measured values for detectors inside the guide tube of the fuel assembly B03.

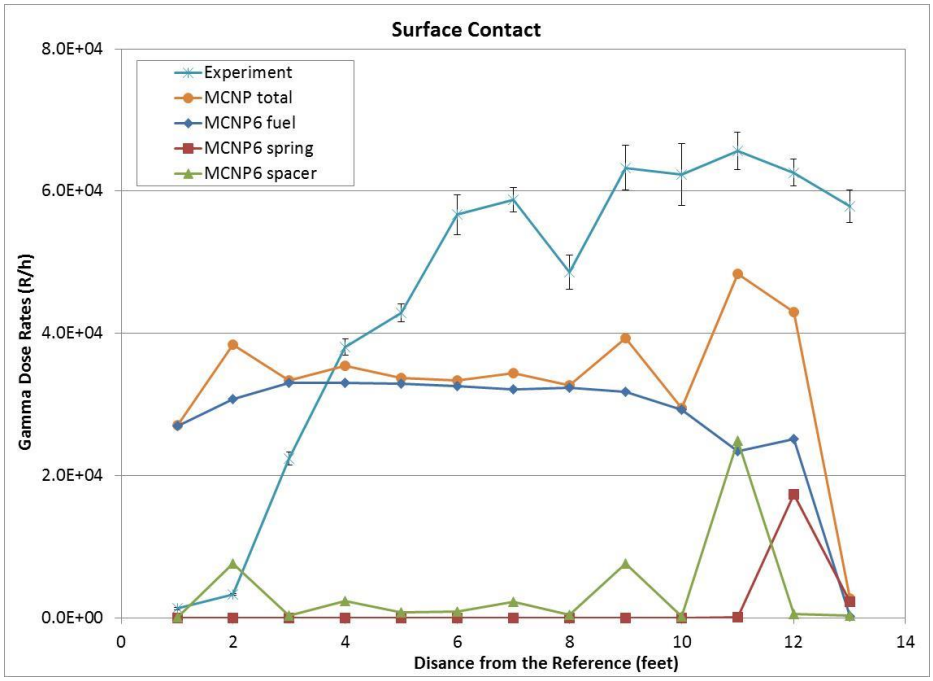

Figure 23 Comparison of the calculated gamma dose rates and the measured values for detectors contacting the B03 fuel assembly surface.

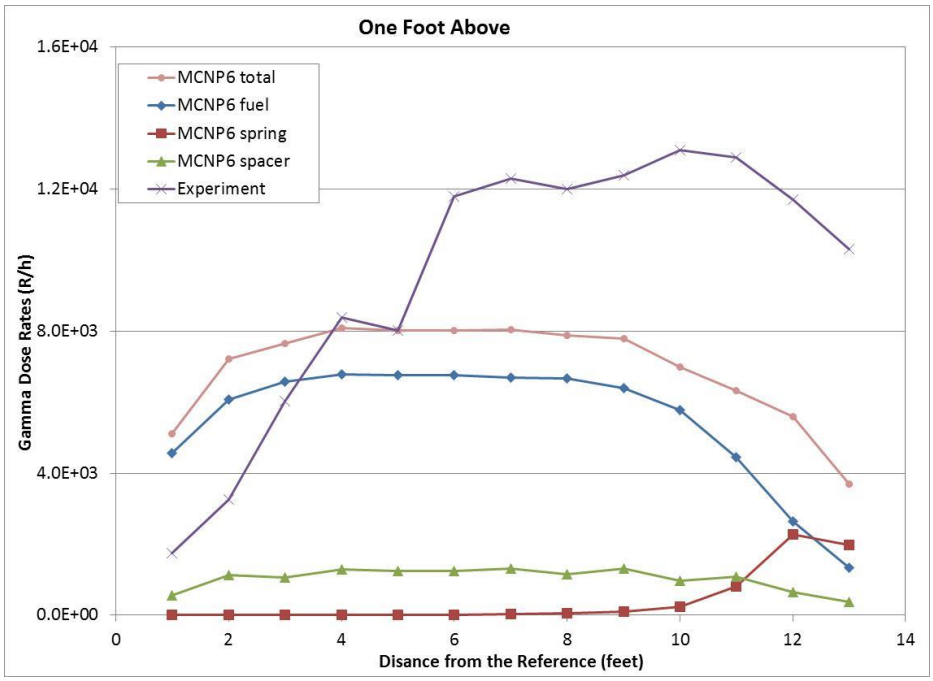

Figure 24 Comparison of the calculated gamma dose rates and the measured values for detectors one foot above the fuel assembly B03.

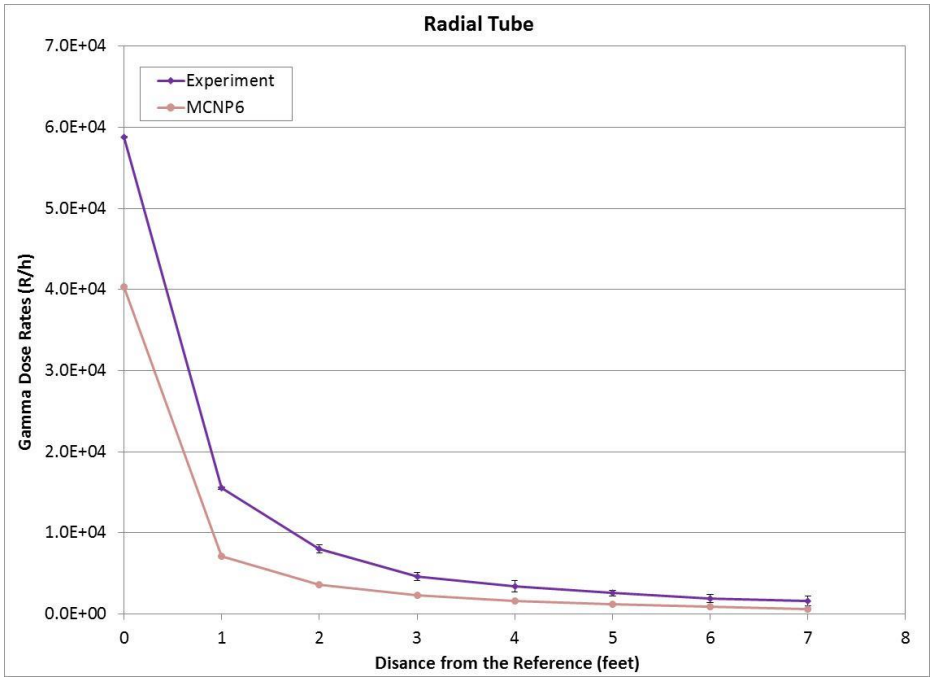

Figure 25 Comparison of the calculated gamma dose rates and the measured values for detectors vertically perpendicular to the fuel assembly B03.

The comparison of the calculated gamma dose rates to the experimental data shows much better agreement for the fuel assembly D04 than for the fuel assembly B03 even though the numerical simulations used the same models for both fuel

assemblies. As shown in Figure 26 to 28, the calculated gamma dose rates and measured values all follow similar shapes as the detectors moved away from the reference points. This observation supports our previous questioning of the accuracy of the experimental data measured or described for fuel assembly B03.

As shown in Figure 26, for detectors hanging about one foot above the fuel assembly, the differences of the calculated gamma dose rates to the experimental data are almost all within or around 10% except the first two detector locations. For detectors on the surface of the fuel assembly as shown in Figure 27, the differences are larger but most of them still within 20%-30% except at the top three detector locations. The numerical simulations have a peak value due to the modeling of the spacer close to the detector that is 11 feet from the fuel assembly bottom reference point. The experimental data have a dip at the detector 4 feet from the bottom. The calculated curve had a dip around 10 feet from the bottom. Based on the numerical simulations shown in Figure 27, these peaks and dips are closely related to the gamma dose rate contributions from the spacers. In our numerical model, the spacer location is read from a general description of the Westinghouse 15X15 fuel assembly. This numerical comparison suggests that the spacer locations or its relative position to the detectors may not be accurate in our numerical model.

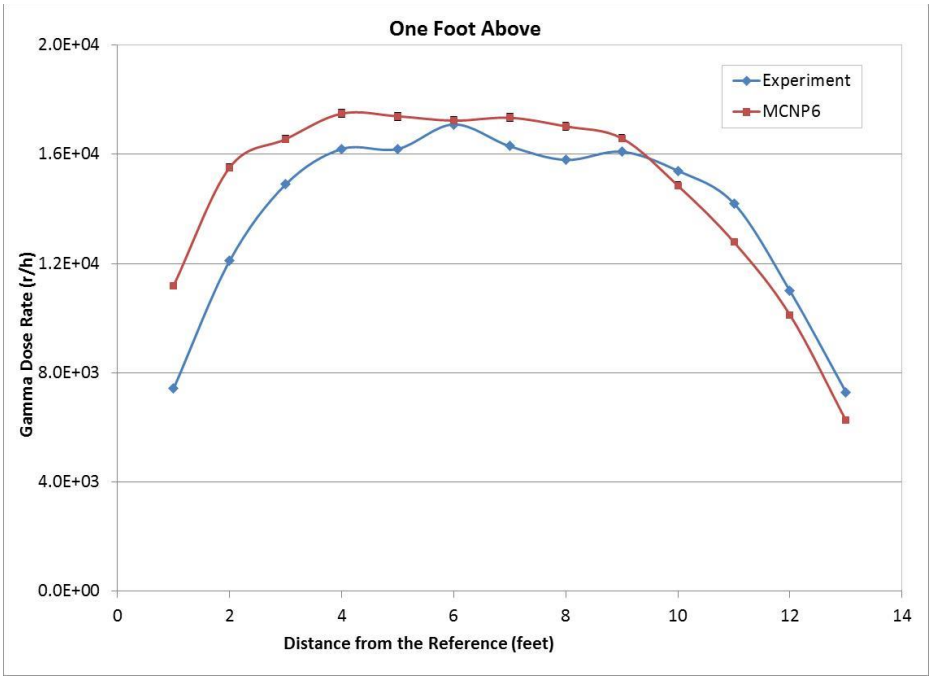

Figure 26 Comparison of the calculated gamma dose rates and the measured values for detectors one foot above the fuel assembly D04.

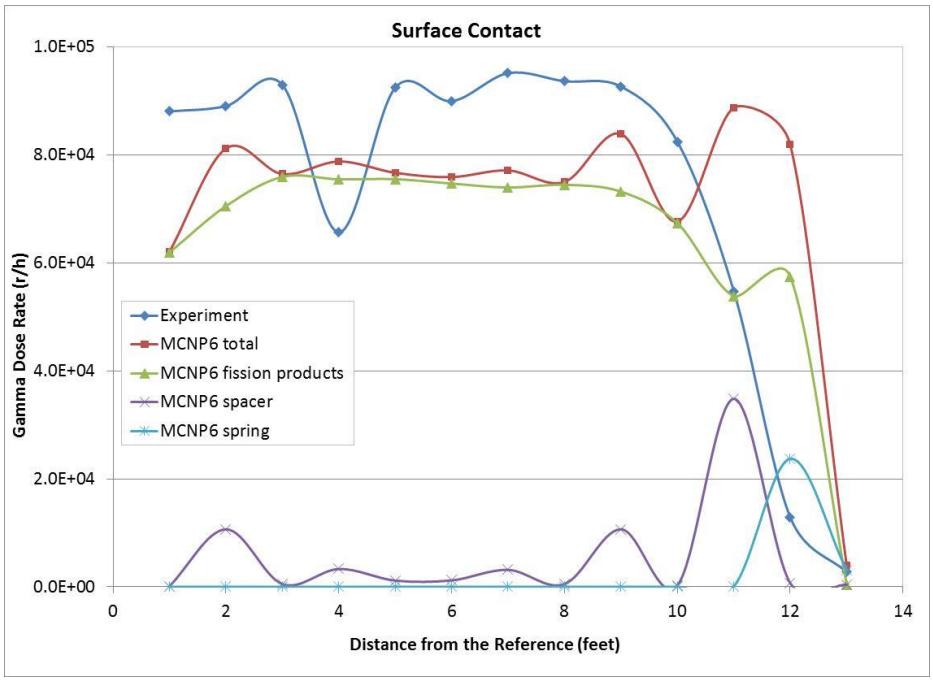

Figure 27 Comparison of the calculated gamma dose rates and the measured values for detectors contacting the D04 fuel assembly surface.

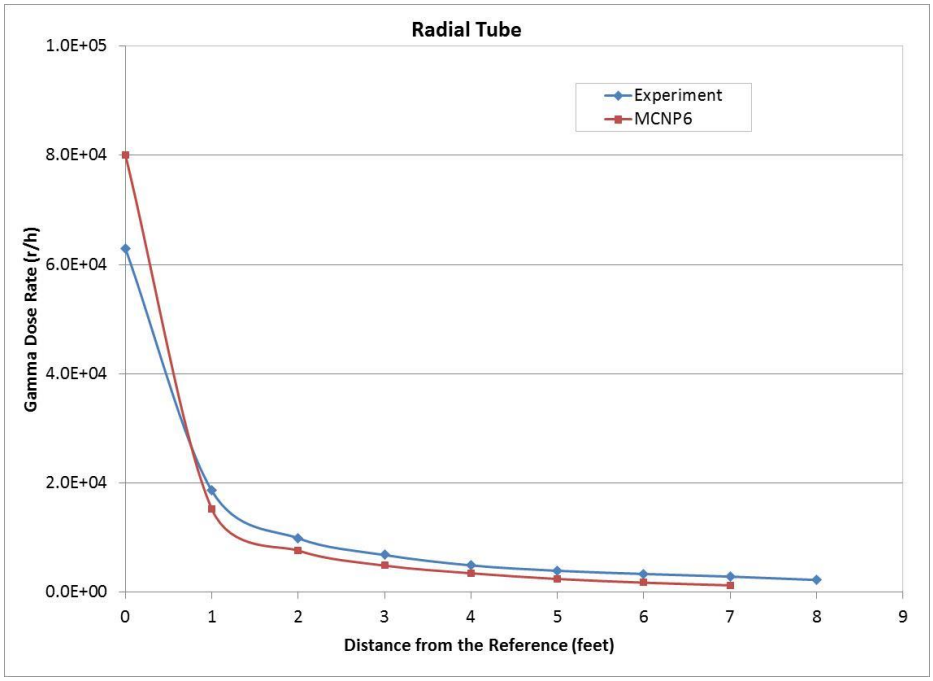

Figure 28 Comparison of the calculated gamma dose rates and the measured values for detectors vertically perpendicular to the fuel assembly D04.

In addition, Figure 28 compares the gamma dose rates in the vertical directions. Except for the first point, the calculated gamma dose rates are all less than their corresponding experimental values. Its differences are increased from 20% to more than 50% as the detectors moved away from the fuel assembly. For the first point, the measured gamma dose rate is 63.0 kR/h. The calculated gamma dose rate from the fuel is 60.4 kR/h. However, in the numerical model, the detector is close to one of the spacers and the calculated gamma dose rate has a large component of about 19.7 from the spacer. This discrepancy also indicated the inaccurate spacer locations in our numerical model.

5. Summary and Future Work

The current dose rate threshold is 100 r/h for a used nuclear fuel assembly to be considered as self-protected. The commercial spent fuel assembly right after discharge from the reactor core is usually self-protected due to its high radioactivity. This radioactivity is virtually all gamma radiation with neutron contributions a few orders of magnitude lower. The radioactivity decreases as the radioisotopes decay. Thus, it is important to calculate accurately the gamma dose rates of the spent fuel assembly at different decay periods to ensure its self-protecting properties remained after periods of cooling and storage. This report described the validation work performed for calculating the gamma dose rates through air from PWR spent nuclear fuel assemblies.

The gamma dose rate measurements using spent nuclear fuel assemblies from the Morris Operation or from the Turkey Point Units were used as the benchmark cases. The numerical simulations have been performed to simulate the two experiments in three steps. To simulate the Morris experiment, MCODE was used to deplete the fresh fuel assembly and to calculate the fuel compositions at discharge. The irradiation of the structural materials inside the core was also simulated to account for the activated cobalt impurities. The ORIGEN-2 code was used to calculate the gamma source released from the discharged fuel assembly. The MCNP6 photon transport simulations were then performed to calculate the gamma dose rates at each detector locations due to the calculated gamma sources.

To simulate the Turkey Point experiment, the SERPENT code was used to perform the fuel depletion calculation as well as to simulate the irradiation of the structural materials. The depleted fuel compositions or irradiated structural materials were input to the ORIGEN-S code which has the updated data libraries and was used to simulate the decay of radioactive isotopes. Three different sets of gamma sources were generated with each representing the gamma rays released from the fission products and fuel, from the irradiated spring, and from the irradiated spacers. In the third step, MCNP6 photon transport simulations were performed to calculate the gamma dose rates at the selected detector locations using each of the gamma sources and flux-to-dose rate conversion factors. The total gamma sources were the sum of the values coming from the three components.

The calculated gamma dose rates were dependent on some of the approximations or assumptions used in the numerical simulations. Sensitivity analyses were performed to determine if the missing details in geometry have a significant impact on the results. Particularly for the Morris experiment, numerical analysis showed that the calculated gamma dose rates away from the fuel assemblies were only weekly dependent on the assumptions of the geometry parameters. The two 1977 and 1991 flux-to-dose conversion factor sets have been both used in the numerical simulations to test their impacts as well. The calculated gamma dose rates using the 1991 conversion factors were chosen to be compared with the experimental data for both benchmark studies since it leads to lower dose rates and are more conservative for evaluating the self-protection abilities of the nuclear fuels. The irradiation of Co-59 impurities inside the structural materials, particularly in the Inconel spacers, was addressed in the numerical simulations. Numerical studies showed that the decay of the irradiation product Co-60 needs to be accounted in calculating the gamma dose rates from fuel that has been discharged within a few years. After several decades, the contribution from Co-60 is insignificant due to its 5.26y half-life. The gamma sources calculated in the decay step were collapsed as multi-group continuous sources. Different axial distributions of these gamma sources inside the MCNP6 photon transport simulations were tested. Numerical simulations showed that the gamma source axial distributions have large impacts on the calculated gamma dose rates at locations close to the top fuel assemblies. The radioactive gamma sources were assumed to follow a similar axial distribution of the fission source. The Wagner fuel burnup distribution for a typical PWR fuel assembly was selected to distribute the gamma sources in the numerical simulations. It was used to distribute the gamma source inside the fuel zone, or among the different spacers for the Turkey Point experiments as well.

For the Morris experiments, the gamma dose rates were calculated at 9 detector locations for four spent fuel bundles named 1A, 2A, 2B, and 2D which were in storage at the Morris Operation facility. Compared with the measured gamma dose rates, the numerical calculations do not overestimate the gamma dose rates at any of the detector locations. The calculated gamma dose rates were conservative in terms of self-protection for this analysis. In particular, the calculated average gamma dose rates for the fuel assembly 2A and 2B consistently agreed with the measured dose rates for all the axial detector locations within an underestimation within 15% at all detector locations. For the other two fuel bundles 1A and 2D, the differences were slightly larger but within 25% for most locations.

The numerical benchmark studies were also performed for two spent fuel assemblies B03 and D04 discharged from the Turkey Point Unit. Much larger deviations were observed between the calculated gamma dose rates and the measured values in this analysis. The numerical simulations were performed consistently using the same models for the two fuel assemblies. However, the numerical simulations have much better agreements with the measurements for fuel assembly D04 than those for B03. In particular, similar axial distributions of the

gamma dose rates inside the experimental tubes were observed between the numerical calculations and the measurements for D04 fuel assembly, but not for B03. The experimental data for B03 are questionable because of the unexplained peaks or shapes significantly different from both the numerical simulations and the corresponding D04 experimental data obtained at the same locations.

The calculated gamma dose rates for D04 fuel assembly showed good agreements within 20% for most of the detectors at the middle of the fuel assemblies, which are the reference measurement points for self-protection purposes. Large differences were found at the top end or bottom end of the fuel assembly locations. These larger differences were usually at positions close to the spacers modeled in the numerical simulations. The calculated dose rates from the different gamma sources were separated in the numerical studies and showed that the spacers may contribute large components to the overall total dose rates when the detector was modeled too close to the spacers. These large discrepancies also indicate the relative positions of the spacers and detectors in the numerical models may not be appropriately described. In addition, unlike in the benchmark studies for the Morris experiments, the calculated gamma dose rates for the D04 fuel assembly were not always smaller than the experimental data, even at those detectors located around the middle of the fuel assembly planes. The amount of cobalt impurities have large impacts on the total gamma dose rates calculated. It is not clear whether the amount of cobalt assumed inside the fuel assemblies are good estimations to the actual concentrations in the Turkey point fuel assemblies. This information was not provided in the experimental descriptions and should be included for all future measurements.

Overall, the benchmark studies performed in this report showed that the numerical methodologies used to calculate the gamma dose rates from the fuel assemblies in the air agreed reasonably well with the measured data with detectors at the middle of the fuel assembly. This indicates that this procedure can be used for self-protection calculations since typical standards require measuring the dose rate at 1 meter away from the axial mid-plane of the fuel assembly. The tested PWR fuel assembly burnup ranged from 25 MWd/kg to 40 MWd/kg and the fuel assembly decay time ranged from 1.8 year to 7 years. The calculated gamma dose rates are affected by many factors, such as the actual impurities inside the materials, the actual fuel burnup of the fuel assemblies, the flux-to-dose conversion factors, etc. The two experimental data sets used in the benchmark studies were performed almost 40 years ago. Similar future benchmark studies using more reliable and high quality experimental data are required to further improve our evaluation of the calculated gamma dose rates from the spent nuclear fuel assembly. Other fuel assemblies with deeper fuel burnups and longer decay times or other types of spent fuel assemblies such BWR fuel assembly or MOX fuel assemblies are also beneficiary for future evaluations.

References

[1] B. Feng, R.N. Hill, R. Girieud, R. Eschbach, “Comparison of Gamma Dose Rate Calculations for PWR Spent Fuel Assemblies,” *The Role of Reactor Physics Toward a Sustainable Future PHYSOR 2014*, The Westin Miyako, Kyoto, Japan, Sep 28 – Oct 3, 2014 (2014).

[2] W.R. Lloyd, M.K. Sheaffer, and W.G. Sutcliffe, “Dose Rate Estimates from Irradiated Light-Water-Reactor Fuel Assemblies in Air,” Lawrence Livermore National Laboratory, Livermore, CA, UCRL-ID-115199 (1994)

[3] H. R. Strickler, K, J. Eger, “In-Plant Test Measurements for Spent Fuel Storage at Morris Operation, Volume 2, Fuel Bundle Radiation Levels,” NEDG—24922-2, Sep 1981 (1981).

[4] C. E. Willingham, “Radiation Dose Rates from Commerical PWR and BWR Spent Fuel Elements,” PNL-3954/UC-70 (1981).

[5] R. B. Davis, “Data Report for the Nondestructive Examination of Turkey Point Spent fuel assemblies B02, B03, B17, B41 and B43,” Hanford Engineering Development Laboratory, HEDL-TME 79-68/UC-70 (1980).

[6] R. Eschbach, B. Feng, etc., “Verification of Dose Rate Calculations for PWR Spent Fuel Assemblies,” Proceedings of GLOBAL 2017 International Nuclear Fuel Cycle Conference, September 24-29, 2017 –Soeul (korea (2017).

[7] Z. Xu, et al. (2006), “MCODE, Version 2.2 – An MCNP-ORIGEN Depletion Program”, MIT technical report, NFC-104.

[8] D. B. Pelowitz, “MCNP6-TM User’s Manual,” LA-CP-11-01708, Dec 2011 (2011).

[9] A. G. Croff, “A User’s Manual for the ORIGEN-2 Computer Code,” ORNL/TM-7175 (1980).

[10] J. Leppanen, “Serpent – a Continuous-energy Monte Carlo Reactor Physics Burnup Calculation Code,” June 18, 2015 (2015).

[11] Americal Nuclear Society, “American National Standard for Neutron and Gamma-Ray Flux-to-Dose-Rate Factors,” ANSI-ANS-6.1.1-1991 (1991).

[12] J. W. Wagner and M. D. DeHard, “Review of Axial Burnup Distribution Considerations for Burnup Credit Calculations,” ORNL/Tm-1999/246 (1999).

[13] W.B. Weihermiller and G. S. Allison, “LWR Nuclear Fuel Bundle Data for Use in Fuel Bundle Handling,” PNL-2575/UC-85 (1979).

[14] R. J. McConn Jr, G. J. Gesh, R. T. Pagh, R. A. Rucker, R. G. Williams III, “Compendium of Material Composition Data for Radiation Transport Modeling,” PIET-43741-TMN-963/PNNL-15870 (2011).

[15] I.C. Gauld, “ORIGEN-S: Depletion Module to Calculate Neutron Activation, Actinide Transmutation, Fission Product Generation and Radiation Source Terms,” ORNL/TM-2005/39 (2011).

Nuclear Science and Engineering Division
Argonne National Laboratory
9700 South Cass Avenue, Bldg. 208
Argonne, IL 60439

www.anl.gov

Argonne National Laboratory is a U.S. Department of Energy
laboratory managed by UChicago Argonne, LLC